



Review

# Recent Progress in Mixed-Matrix Membranes for Hydrogen Separation

Chong Yang Chuah <sup>1,†</sup> , Xu Jiang <sup>1,†</sup>, Kunli Goh <sup>1</sup>  and Rong Wang <sup>1,2,\*</sup>

<sup>1</sup> Singapore Membrane Technology Centre, Nanyang Environment & Water Research Institute, Nanyang Technological University, Singapore 637141, Singapore; chongyang.chuah@ntu.edu.sg (C.Y.C.); xu.jiang@ntu.edu.sg (X.J.); gohkunli@ntu.edu.sg (K.G.)

<sup>2</sup> School of Civil and Environmental Engineering, Nanyang Technological University, Singapore 639798, Singapore

\* Correspondence: rwang@ntu.edu.sg

† These authors contributed equally to this work.

**Abstract:** Membrane separation is a compelling technology for hydrogen separation. Among the different types of membranes used to date, the mixed-matrix membranes (MMMs) are one of the most widely used approaches for enhancing separation performances and surpassing the Robeson upper bound limits for polymeric membranes. In this review, we focus on the recent progress in MMMs for hydrogen separation. The discussion first starts with a background introduction of the current hydrogen generation technologies, followed by a comparison between the membrane technology and other hydrogen purification technologies. Thereafter, state-of-the-art MMMs, comprising emerging filler materials that include zeolites, metal-organic frameworks, covalent organic frameworks, and graphene-based materials, are highlighted. The binary filler strategy, which uses two filler materials to create synergistic enhancements in MMMs, is also described. A critical evaluation on the performances of the MMMs is then considered in context, before we conclude with our perspectives on how MMMs for hydrogen separation can advance moving forward.

**Keywords:** mixed-matrix membrane; zeolite; metal-organic framework; covalent organic framework; graphene; hydrogen separation



**Citation:** Chuah, C.Y.; Jiang, X.; Goh, K.; Wang, R. Recent Progress in Mixed-Matrix Membranes for Hydrogen Separation. *Membranes* **2021**, *11*, 666. <https://doi.org/10.3390/membranes11090666>

Academic Editor: Sergey Shishatskiy

Received: 29 July 2021

Accepted: 25 August 2021

Published: 30 August 2021

**Publisher's Note:** MDPI stays neutral with regard to jurisdictional claims in published maps and institutional affiliations.



**Copyright:** © 2021 by the authors. Licensee MDPI, Basel, Switzerland. This article is an open access article distributed under the terms and conditions of the Creative Commons Attribution (CC BY) license (<https://creativecommons.org/licenses/by/4.0/>).

## 1. Introduction

The global energy landscape is changing at a rapid pace, driven by the ever burgeoning world's population and increasing demand from economic growth [1]. Today, the global energy outlook is also shaped by climate change and emerging opportunities from renewable energy [2,3]. Hydrogen (H<sub>2</sub>), at the crossroad between electricity and fuel, as well as long-term energy storage and potential low-carbon energy resource, is envisaged to play an important role in our efforts toward decarbonization and sustainability. However, being an energy carrier and not an energy source, hydrogen has to be first produced from primary energy sources that inevitably involve fossil fuel [4]. Hence, to enable hydrogen as a low-carbon energy resource, two approaches are at present widely undertaken and researched upon: (1) leveraging renewable electricity to drive an electrolysis process, which produces hydrogen (termed as green hydrogen) from water [5,6], and (2) cleaning the carbon emissions from hydrogen produced from natural gas to yield blue (decarbonized) hydrogen by means of carbon capture, storage and utilization (CCSU) [6–8]. As of 2020, green hydrogen is costly to produce, which is priced between USD 3.00–6.55 per kg hydrogen, due to the limited electrolysis capacity and the high cost of tapping on renewable energy [9]. Blue hydrogen, however, is relatively cheaper at USD 1.40–2.40 per kg hydrogen, but is heavily subjected to price fluctuation from the natural gas market, and the cost to implement CCSU technologies [10]. Notwithstanding both technological and cost

constraints, the general consensus is that blue hydrogen will remain as the most attractive and viable option in the foreseeable future [11].

Membrane separation is a compelling technology for hydrogen purification and supporting CCSU efforts for blue hydrogen generation, owing to its cost-effectiveness, energy efficiency and modular design that favors easy retrofitting to existing plants [12–15]. The key driver of this technology is the gas separation membranes, which are currently well-represented by polymeric membranes and limited by a recurring permeability–selectivity tradeoff in performances [16–18]. Hence, in this review, we focus on one of the most extensively used and important strategies to overcoming this tradeoff, the mixed-matrix membrane (MMM) strategy. To begin the discussion, we first highlight the key technologies for today’s hydrogen generation. Then, under this background, we compile different separation technologies for hydrogen purification, comparing membrane technology to pressure-swing adsorption (PSA) and cryogenic distillation, as well as discussing their pros and cons. Thereafter, we summarize recent progress in MMMs (mostly in the last 10 years) for hydrogen separation, focusing especially on emerging filler materials, including zeolites, metal-organic frameworks (MOFs), covalent-organic frameworks (COFs) and graphene-based materials. Finally, we provide an overview of the binary filler strategy, which uses two filler materials to create synergistic enhancements, before giving a critical evaluation on the separation performances of MMMs and sharing our perspectives to help pave future efforts in this area of research.

## 2. Current Hydrogen Generation Market and Challenges

Hydrogen is not an extractable resource, but created via synthetic means and separated from other elements before producing in its pure form [19]. Essentially, steam-methane reforming (SMR), partial oxidation (POX), gasification and electrolysis are currently the mainstream technologies available for hydrogen generation, with a market share of 48%, 30%, 4% and 18%, respectively, as cited in 2012 [20]. These technologies typically rely on the utilization of non-renewable fossil fuels (e.g., natural gas, coal and fuel oil) for hydrogen generation [21,22]. In 2018, it was reported that about 75% of the global hydrogen production (ca. 70 million tons) derived from the use of natural gas, which accounted for approximately 6% of the global natural gas supply [23,24]. In this section, a brief outline of each technology will be discussed (Figure 1).

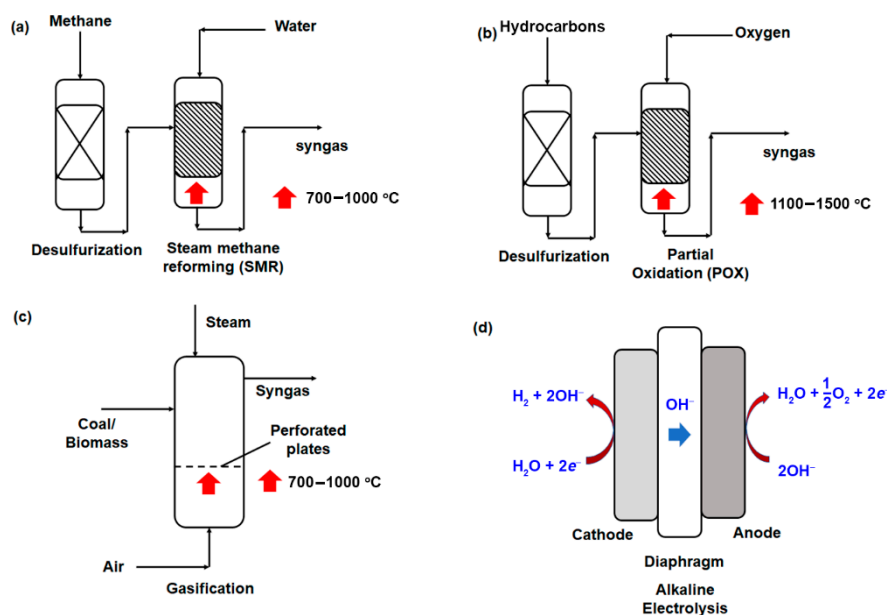
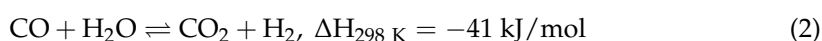
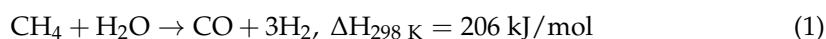
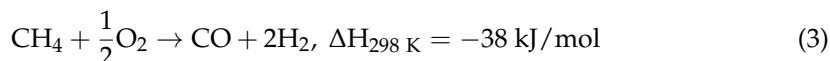


**Figure 1.** Methods to generate hydrogen gas from the feed (a) steam methane reforming (SMR), (b) partial oxidation (POX), (c) gasification, and (d) alkaline electrolysis. Reprinted with permission from Ref. [25], Creative Commons license CC BY 4.0.

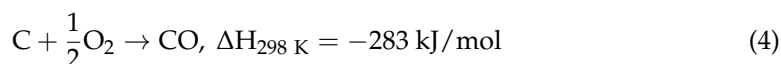
First, SMR is a matured technology that utilizes high-temperature steam (ca. 700–1000 °C) to produce hydrogen from natural gas comprising mainly methane gas. The produced syngas has H<sub>2</sub> and CO in the stoichiometric ratio of 3:1 (Equation (1)), which due to the endothermicity of the reaction, has resulted in the need for high operating temperature and steam-to-methane ratio of ca. 2.5–3.0 to minimize the formation of carbonaceous material (coke) [25]. CO molecules that are generated can be further converted to additional H<sub>2</sub> by a water-gas shift (WGS) reaction as illustrated in Equation (2). Despite SMR being widely used today, the large CO<sub>2</sub> emission, amounting to 830 million tons annually, is a major drawback in light of the current concern over global warming and climate change [19,23]. Thus, downstream carbon capture, sequestration and utilization are an important piece of the puzzle in realizing blue hydrogen production by SMR technology.



POX, however, creates syngas through the mixing of hydrocarbon fuel under sub-stoichiometric manner. As compared to SMR, this reaction occurs at a higher reaction temperature (1100–1500 °C) [26]. Considering that the reaction is exothermic, the reaction system can be built in a more compact manner, given that heat exchange is no longer required to maintain the operating temperature. The use of a catalyst is also an option to reduce the reaction temperature to between 600–900 °C and increase the hydrogen yield [26]. In recent years, there is increased use of oxygen enriched air to improve the heating value of the produced syngas [26]. Nevertheless, the syngas produced by POX has in general less hydrogen per unit of input fuel as compared to SMR, based on the stoichiometric chemical equation as provided in Equation (1) and (3) [27]. Besides, effective heat recovery is often challenging due to higher reaction temperature.



Gasification is another technology for the generation of syngas. It is an indirect combustion process at an elevated temperature to achieve complete combustion of raw materials at a sub-stoichiometric amount of oxidants [28]. Typically, solid fuels such as coal are used. Biomass is also gaining traction as a feedstock in recent years, owing to the acceleration of waste-to-energy initiatives that drive a circular economy. In comparison to the previous two approaches, the production of syngas via gasification requires the incorporation of both oxygen and steam as illustrated in Equation (3) and (4), respectively. Similar to POX, the heating value of the produced syngas from gasification can be enhanced by the use of oxygen-enriched air, although the overall energy efficiency is comparatively lower (35–50%) compared to POX system (70–80%) [20].



Last but not least, as discussed in the introduction, electrolysis is a process that uses electric current to split water molecules into hydrogen and oxygen molecules. Alkaline water electrolysis (AWE) is the most common approach to generate hydrogen, which involves the use of two electrodes—separated by a diaphragm to selectively allow hydroxide ion transport only in liquid alkaline electrolyte solution such as potassium hydroxide (KOH) or sodium hydroxide (NaOH) solution [29]. Among the four different technologies, AWE operates at the lowest operating temperature of between 30–80 °C with the concentration of the electrolyte typically in the range of 20–30% [30,31]. Recently, the use of proton exchange membrane (PEM) electrolysis in which the diaphragm used are typically composed of solid polysulfonated membrane (e.g., Nafion<sup>®</sup>, fumapen<sup>®</sup>) to allow proton (H<sup>+</sup>) transport, has been proposed as a viable alternative [32]. Notwithstanding the higher overall energy efficiency of 60–80%, electrolysis suffers from short technical lifetime (ca. 40,000 h) [20]

and small production scale, which both hinder its adoption and eventual replacement of the conventional SMR as a mainstream hydrogen production technology. Besides, in the near future, the electricity used to power the electrolysis process will continue to derive from nonrenewable primary sources (e.g., fossil fuels), which results in not only inevitable negative environmental impacts, but also regressing to unsustainable practices.

### 3. Hydrogen Purification: Membrane vs. Other Technologies

All the aforementioned technologies do not produce pure hydrogen, which entails the need for purification to create hydrogen of targeted purity for its desired downstream applications. The common impurities associated with each hydrogen generation technology are summarized in Table 1. To date, pressure swing adsorption (PSA), cryogenic distillation and membrane-based separation are current technologies for hydrogen purification (Figure 2) in which key attributes will be elaborated in this section. We believe such discussions will be useful for readers to comprehend how membrane-based separation is different from the conventional PSA and cryogenic distillation.

**Table 1.** Hydrogen from different generation technologies and its common impurities [33].

Hydrogen Generation Technology	Common Impurity
Steam methane reforming	CO, CO <sub>2</sub> and CH <sub>4</sub>
Partial oxidation of hydrocarbons	CO, CO <sub>2</sub> and CH <sub>4</sub>
Gasification (coal/oil/biomass)	Light hydrocarbons, CO, CO <sub>2</sub> , CH <sub>4</sub> , O <sub>2</sub> , and N <sub>2</sub>
Electrolysis of water	CH <sub>4</sub> , O <sub>2</sub> , N <sub>2</sub> , CO <sub>2</sub> , and CO

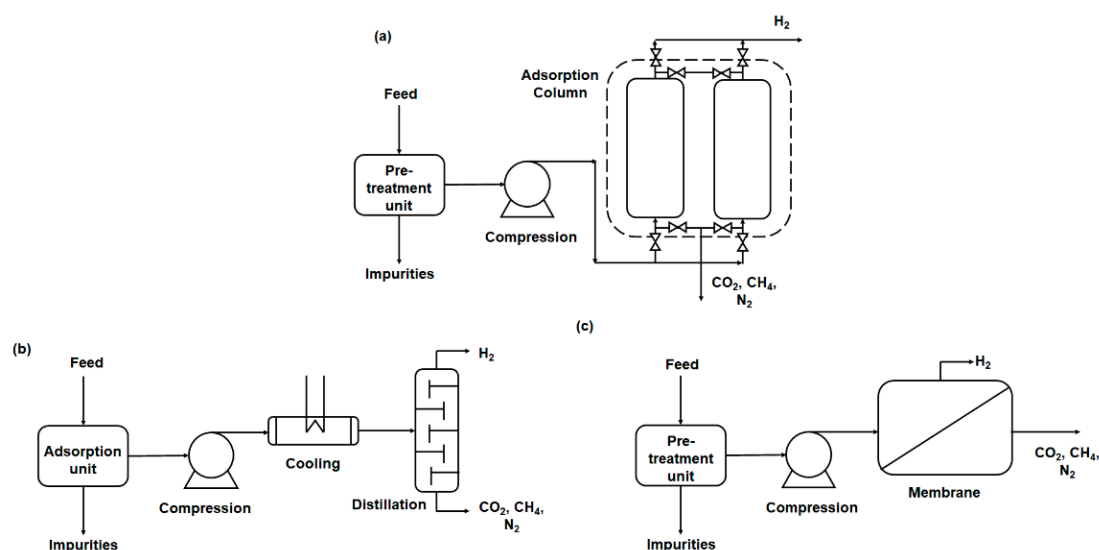


**Figure 2.** Illustration of (a) pressure swing adsorption (PSA), (b) cryogenic distillation, and (c) membrane-based separation. Reprinted with permission from ref. [34]. Copyright 2020 Elsevier.

PSA is the industrial standard for hydrogen purification. It has been reported that at least 85% of the current global hydrogen production units are dominated by the PSA technology [35] in which largescale production capacity up to 400,000 Nm<sup>3</sup>/h has been successfully developed by the Linde group [36]. PSA involves the utilization of micro- and mesoporous solid adsorbents (e.g., zeolites, activated carbons, alumina and silica gels) that are packed in an adsorption column for separation. Due to the small polarizability and quadrupole moment of hydrogen gas in comparison to other impurities such as carbon dioxide (CO<sub>2</sub>), nitrogen (N<sub>2</sub>) and methane (CH<sub>4</sub>), a pressurized gas feed up to 40 bar is necessary to induce effective adsorption of polarizable gas impurities by the adsorbents [19,37]. High-pressure hydrogen, which cannot be adsorbed, will be recovered at the top of the adsorption columns. In general, PSA possesses the capability to achieve

high hydrogen purity (99.999%) [38], albeit a typical 65–90% hydrogen recovery [16]. Besides, PSA operates on a cyclic basis to regenerate spent adsorbents for subsequent adsorption process. Thus, PSA operation is comparatively economical if high input gas and high flow rate are utilized in the process [35,38].

Conversely, cryogenic distillation purifies based on boiling point differences. Hydrogen has the lowest boiling point ( $-252\text{ }^{\circ}\text{C}$  at 1 bar pressure), and thus the most undesirable impurities can be condensed into a liquid phase and separated from the targeted hydrogen [39]. Cryogenic distillation offers higher handling capacity with higher hydrogen recovery, but at the same time, higher cost incurs from gas compression at cold operating condition, and lower purity level of the extracted hydrogen than PSA, with the highest purity reported at 99% [38]. Hence, a hybrid system combining PSA and cryogenic distillation is proposed in which the waste gas from the PSA operation (with high  $\text{CO}_2$  content) is sent to cryogenic distillation for further hydrogen extraction [40]. Such an approach is currently adopted by Airliquide under the tradename CryoCap<sup>TM</sup>  $\text{H}_2$  technology [41]. As cryogenic distillation operates at a low temperature, purified hydrogen can be readily stored in liquid phase, allowing for a more efficient transportation as compared to pressurized hydrogen gas. Cryogenic distillation, similar to PSA, is competitive only at large-scale operation and when the feed gas hydrogen concentration is low [34].

As compared to PSA and cryogenic distillation, hydrogen purification by membrane-based separation is competitive in its own right and is considered a potential tool to generate hydrogen-enriched gas stream [42,43]. Membrane separates via a difference in the gas permeation rates between hydrogen and other impurities, which is dictated mainly by a solution-diffusion mechanism [16,17]. In the solution-diffusion mechanism, the permeability of a gas is a product of its diffusivity and solubility [44]. Hydrogen has a higher diffusivity, as it can diffuse faster than other gas constituents, considering that hydrogen molecules possess a small kinetic diameter [45]. Nonetheless, due to its small polarizability, the solubility of hydrogen in a membrane is considerably lower than other polarizable gases such as  $\text{CO}_2$  [19]. Thus, understanding the mass transport mechanism is critical to the success of membrane-based hydrogen separation. Unlike PSA and cryogenic distillation, membrane-based separation can be more energy-efficient and cost-effective. This is attributed to the feasibility of membranes to perform gas separation without a phase change or desorption process, which is needed in cryogenic distillation and PSA [46,47]. In addition, it requires lower capital investments due to ease of retrofitting and smaller footprint. Thus, membrane-based separation is able to value-add in areas not possible by the other two technologies. However, the membrane technology is also limited to a smaller feed stream flow rate, moderate hydrogen purity output (90–95%) and lower overall recovery rate (85–90%) [48].

At present, polymeric membranes have a dominant presence in the membrane market for hydrogen separation, owing to the suitability and economical large-scale processing of polymeric materials into separation membranes. However, given the solution-diffusion mechanism as driven by their dense membrane structures, polymeric membranes continue to be challenged by the permeability-selectivity tradeoff in all industrially relevant gas pairs ( $\text{H}_2/\text{CO}_2$ ,  $\text{H}_2/\text{CH}_4$  and  $\text{H}_2/\text{N}_2$ , see Figure 3). Hence, one primary focus is on resolving this tradeoff issue in hydrogen separation membranes. Among the many different types of membranes, including (nano)laminated and thin-film (nano)composite membranes that are studied to date [49–51], MMMs are one of the most well-researched and promising approaches [52,53]. Defined as the incorporation of filler materials into continuous polymer matrices, MMMs have the clear objective of capitalizing filler materials to tune the transport properties of the polymer matrices. In this regard, filler materials, such as zeolites, MOFs, COFs, and graphene-based materials, will be covered in this review. While there are other filler materials such as carbon nanotubes, which have been adopted for hydrogen separation [54,55], these filler materials are emerging and gaining importance in recent years. Binary filler strategy using these fillers is also at times prepared to create synergistic performance enhancements. For these reasons, in the following section, we delve into this



exciting field of research, discussing current state-of-the-art MMMs that contain these filler materials, their merits and limitations, as well as effects on the membrane performances for hydrogen separation.

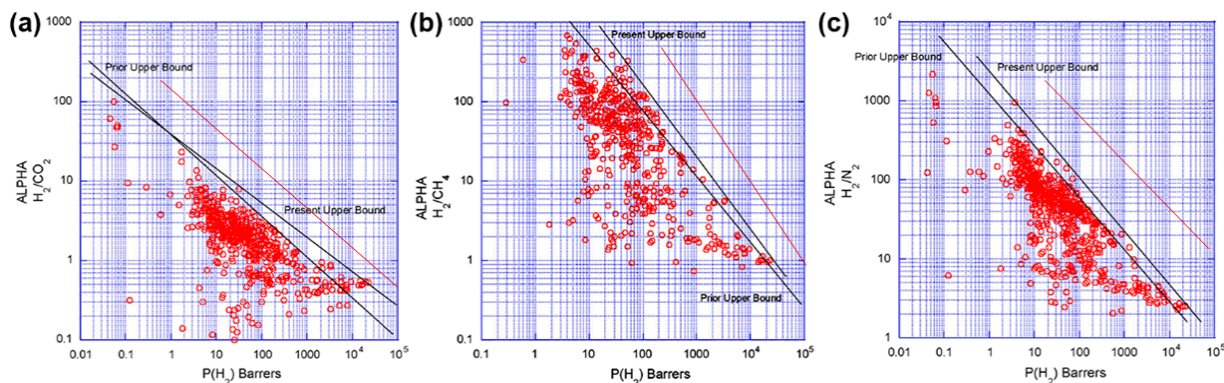


**Figure 3.** Robeson plot showing the present (2008) and prior (1991) upper bound for (a)  $\text{H}_2/\text{CO}_2$ , (b)  $\text{H}_2/\text{CH}_4$ , and (c)  $\text{H}_2/\text{N}_2$  gas pairs. Additional line in brown represents the most well-received upper bounds based on up-to-date profiles obtained from the following references [56–58]. Reprinted with permission from ref. [17]. Copyright 2008 Elsevier.

#### 4. Mixed-Matrix Membranes for Hydrogen Separation

##### 4.1. Zeolite-Based Membranes

**Zeolites** are microporous crystalline aluminosilicates, which are interconnected via  $\text{SiO}_4$  and  $\text{AlO}_4$  tetrahedron primary units. As a group of inorganic microporous materials, zeolites have been widely studied for gas storage and separation due to their large specific area and excellent physicochemical stability [59–63]. Zeolites can be synthesized in different shapes, particle sizes, and pore diameters for various gas separation applications. For  $\text{H}_2$  separation, MMMs can either be  $\text{H}_2$ -selective or reverse-selective, depending on the polymer and zeolite selection [64]. For example, MFI, SAPO-34, and SSZ-13 are  $\text{CO}_2$ -selective zeolites, owing to the  $\text{CO}_2$  favored competitive adsorption [64–66]. Hu et al. reported a MMM consisted of Pebax<sup>®</sup>1657, ionic liquid (IL), and surface modified SAPO-34 [67]. The SAPO-34 was decorated with  $-\text{NH}_2$  groups to enhance its interfacial compatibility with the polymer matrix. The presence of IL elevates the  $\text{CO}_2$  affinity, resulting in a high  $\text{CO}_2/\text{H}_2$  selectivity of 22.1 (Table 2) [67].

Most of the zeolites are adopted for  $\text{H}_2$ -selective membranes due to molecular sieving effect by their narrow pores. For example, in Matrimid<sup>®</sup> 5218/DDR zeolite MMMs, the appropriate pore size of DDR zeolite ( $3.6 \times 4.4 \text{ \AA}$ ) played a crucial role in achieving a high  $\text{H}_2/\text{CH}_4$  selectivity of 129.8 since the pore diameter falls in between the diameter of  $\text{H}_2$  ( $2.9 \text{ \AA}$ ) and  $\text{CH}_4$  ( $3.8 \text{ \AA}$ ) [68]. Similarly, zeolite 4A with pore diameter of  $3.8 \text{ \AA}$  was also found to be able to significantly enhance the  $\text{H}_2/\text{N}_2$  and  $\text{H}_2/\text{CH}_4$  selectivity of its MMMs [69,70]. To overcome the interfacial compatibility issue, Esmaili et al. adopted nanosizing and silanization strategies to increase interfacial interaction between zeolite 4A and polyvinyl acetate (PVAc), as to reduce zeolite 4A agglomeration in MMMs, leading to better filler dispersion and increase in  $\text{H}_2$  selectivity [71]. A recent study by Eden et al. also saw the use of hydroxyl sodalite with a cage structure and small pore diameter of  $2.6 \text{ \AA}$  [72]. By infusing 10 wt.% of hydroxy sodalite filler in PSF matrix, a huge increase in  $\text{H}_2$  permeance from  $2.7 \times 10^{-9} \text{ mol m}^{-2} \text{ s}^{-1} \text{ Pa}^{-1}$  to  $7.3 \times 10^{-9} \text{ mol m}^{-2} \text{ s}^{-1} \text{ Pa}^{-1}$  was observed under single gas evaluation (Table 2). This was accompanied by a superior  $\text{H}_2/\text{CO}_2$  selectivity of 54.9 when tested under mixed-gas evaluation [72].

On a different note, spherical particles of ordered mesoporous silica have strong capacity to minimize filler agglomeration when used in MMMs, owing to the spherical shape and lower surface area to volume ratio [73–75]. For example, Tseng et al. reported a series of SBA-15-derived MMMs containing SBA-15 particles of different shapes and sizes and found that a spherical shape with particle diameter of  $1.6 \mu\text{m}$  had the best compatibility

with the polymer matrix [76]. To reduce the pore diameter of the mesoporous silica to a range suitable for H<sub>2</sub> separation, Zornoza et al. revealed a layer-by-layer (LBL) procedure to synthesize silicalite-1 crystals over the spherical silica, giving rise to hollow zeolite spheres (HZSs) (Figure 4) [77,78]. The HZSs were used as filler materials in polysulfone (PSF) and Matrimid® 5218 and 6FDA-DAM matrices. At 8 wt.% loading, H<sub>2</sub> permeability could reach 15, 38 and 541 barrer, with H<sub>2</sub>/CH<sub>4</sub> selectivity of 80, 180 and 25, respectively (Table 2) [77,78]. The enhanced H<sub>2</sub> permeability was attributed to the hollow spheres, giving rise to low transport resistance and higher free volume as a result of the disruption to the polymer chains. More importantly, the silicalite-1 shell offered a regular pore diameter of ~5.5 Å and increased surface roughness of the hollow spheres, leading to improved polymer-filler interfacial interaction and enhanced H<sub>2</sub>/CH<sub>4</sub> selectivity.

**Table 2.** Summary of representative performances for zeolite-based membranes in H<sub>2</sub>-based separation.

Membrane		Separation Performance						Ref.
Filler	Polymer/Support	Test Condition	Permeation Area (cm <sup>2</sup> )	P(H <sub>2</sub> ) (GPU)	Selectivity			
					H <sub>2</sub> /CO <sub>2</sub>	H <sub>2</sub> /CH <sub>4</sub>	H <sub>2</sub> /N <sub>2</sub>	
IL/SAPO-34 (1:4)	Pebax <sup>®</sup> MH1657/PEGDME with ceramic	1 bar, 20 °C	-	4.9 (+188%)	0.11 (+31%)	1.2 (+9%)	-	[67]
IL/SAPO-34-NH <sub>2</sub> (1:4)	Pebax <sup>®</sup> MH1657/PEGDME with ceramic	1 bar, 20 °C	-	2.2 (+29%)	0.05 (−17%)	1.9 (+73%)	-	[67]
IL/SAPO-34-NH <sub>2</sub> (1:2)	Pebax <sup>®</sup> MH1657/PEGDME with ceramic	1 bar, 20 °C	-	2.3 (+35%)	0.05 (−17%)	2.6 (+136%)	-	[67]
SAPO-34	Pebax <sup>®</sup> MH1657/PEGDME with ceramic	1 bar, 20 °C	-	1.5 (−12%)	0.06 (0%)	1.4 (+27%)	-	[67]
DD3R (20 wt%)	Matrimid <sup>®</sup> 5218	1 bar, 25 °C	11.95	34.9 <sup>a</sup> (+105%)	-	375 (+188%)	-	[68]
Zeolite 4A (25 wt%)	PVAc	-	2.3–2.5	3.8 <sup>a</sup> (−36%)	1.6 (−20%)	-	156 (+42%)	[69]
Zeolite 4A (15 wt%)	PVAc	0.75 bar, 30 °C	-	5.8 <sup>a</sup> (0%)	5.3 (+13%)	-	117 (+22%)	[71]
Modified zeolite 4A (15 wt%)	PVAc	0.75 bar, 30 °C	-	5.6 <sup>a</sup> (−3%)	6.1 (+30%)	-	143 (+49%)	[71]
Hydroxyl sodalite (5 wt%)	PSF	-	-	21.8 (+169%)	1.1 (−78%)	-	1.1 (−78%)	[72]
Silica sodalite (15 wt%)	PSF	-	-	22.8 (+182%)	1.1 (−78%)	-	1.0 (−80%)	[72]
HZS (8 wt%)	6FDA-DAM	2 bar, 35 °C	28	541 <sup>a</sup> (+13%)	0.77 (−3%)	25 (+47%)	21 (+62%)	[78]

<sup>a</sup> Permeability reported in the units of barrer; numbers in the parentheses represent the percentage enhancements with respect to the pristine polymeric membranes. 6FDA, 4,4'-(hexafluoroisopropylidene)diphthalic anhydride; DAM, 2,4,6-triphenyl-m-phenylenediamine; PEGDME, poly(ethylene glycol) dimethyl ether; PSF, polysulfone; PVAc, polyvinyl acetate.

Generally, the pore size of most zeolites is too large for a highly efficient H<sub>2</sub> molecular sieving from other gases, especially for H<sub>2</sub>/CO<sub>2</sub> separation. For instance, well-known zeolitic structures, such as MFI, CHA, LTA and FAU (notation defined based on International Zeolite Association, IZA), that are commonly used for post-combustion CO<sub>2</sub> capture possess pore size of 3.8 Å, 3.8 Å, 4.8 Å and 7.4 Å, respectively, which are considerably larger with respect to the kinetic diameter of H<sub>2</sub> molecules (2.9 Å) [44]. Hence, there is limited research focusing on zeolite-based MMMs for H<sub>2</sub> separation. However, in recent

years, emerging advanced nanomaterials, such as MOFs and COFs with narrower and more orderly channels as well as diverse chemical properties, have become a more popular choice for achieving high-performance MMMs for H<sub>2</sub> separation.

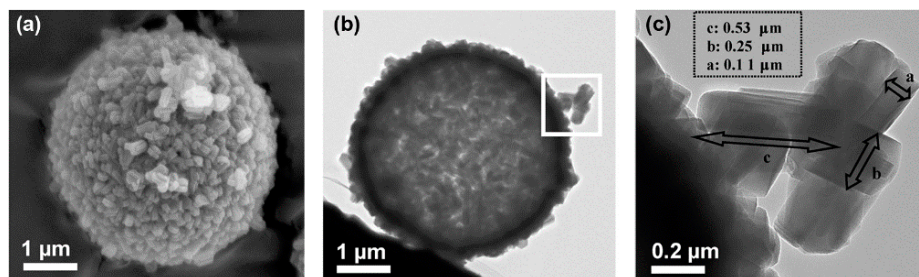


**Figure 4.** Structural morphology of HZSs, showing the (a) scanning electron microscopic (SEM), (b) transmission electron microscopic (TEM) images, and (c) the silicalite-1 crystals on the shell of the hollow sphere. Reprinted with permission from ref. [77]. Copyright 2011 Elsevier.

#### 4.2. MOF-Based Membranes

Compared to the pure inorganic zeolites, MOFs are a group of porous organic-inorganic hybrid materials consisting of metal ions/clusters and rigid organic ligands [79]. The ultrahigh specific areas, adjustable micropore structures, and easily modified surface chemical properties endow MOFs with excellent gas adsorption and molecular sieving abilities, which are attractive for gas separation membranes in recent decades [80,81].

Similar to any other MMMs, the good interfacial compatibility of MOF nanoparticles and polymer matrix is the key prerequisite for better gas separation performance [82,83]. By utilizing functionalized ligands, MOFs could be easily decorated with functionalities such as  $-OH$ ,  $-NH_2$ , and  $-NO_3$  via bottom-up approaches, thereby improving their compatibility with the organic polymers. Cao et al. adopted  $NH_2$ -functionalized CAU-1- $NH_2$  as the filler for poly(methyl methacrylate) (PMMA) membranes [84]. The hydrogen bonds between CAU-1- $NH_2$  and PMMA led to a compact and stable MMMs with an ultrahigh H<sub>2</sub> permeability ( $>1 \times 10^4$  barrer) and a good H<sub>2</sub>/CO<sub>2</sub> selectivity ( $>10$ ) (Table 3) [84]. Hu et al. reported a high selective UiO-66(Hf)-(OH)<sub>2</sub>/polybenzimidazole (PBI) MMM with an excellent H<sub>2</sub>/CO<sub>2</sub> selectivity of 19.4 [82]. Ma et al. also used UiO-66-(OH)<sub>2</sub> as filler for a PI matrix. The obtained UiO-66-(OH)<sub>2</sub>/PI MMMs exhibited a H<sub>2</sub> permeability of up to 907 barrer and a H<sub>2</sub>/CH<sub>4</sub> selectivity up to 42 [85]. Apart from these examples, several other functionalized MOFs, such as MIL-53- $NH_2$  [86,87] and UiO-66- $NH_2$  [88,89], were also demonstrated.

Post-synthetic modification is another promising approach to modifying MOF particles toward better separation performances [90–94]. Al-Maythaly et al. performed a linker exchange of benzimidazolate to benzotriazolate for ZIF-7 nanoparticles to tune the performance of ZIF-7/poly(ether imide) (PEI) membranes [95]. The resulting membranes with post-synthetically modified ZIF-7 filler displayed the highest gas permeability for all test gases with a H<sub>2</sub> permeability of 2021 barrer. Sánchez-Láinez et al. also obtained ZIF-93/11 hybrid nanoparticles by immersing synthesized ZIF-93 particles into benzimidazole solution [96]. The hybrid ZIF-93/11 particles were then applied as a filler for PBI-based MMMs, leading to H<sub>2</sub> permeability of 207 barrer and H<sub>2</sub>/CO<sub>2</sub> selectivity of 7.7 at a high operating temperature of 180 °C.

Alternative to modifying the filler materials, post-synthetic engineering of the membrane formation process can also help to resolve the polymer-filler interfacial challenge. Kim et al. found that post-synthetic thermal-rearrange (TR) could effectively alleviate the interfacial voids between ZIF-8 nanoparticles and TR-polymers [97]. With a 90% TR conversion and 20 wt.% ZIF-8 loading, the MMM reached a H<sub>2</sub> permeability of 1206 barrer with a H<sub>2</sub>/N<sub>2</sub> selectivity of 21.3 (Table 3). Furthermore, Xiang et al. developed a H-bonding assisted LbL assembling strategy to synthesis MMMs, containing phenyl acetyl functionalized MOFs with poly(acrylic acid) (PAA) [98]. Owing to the strong filler-matrix interaction,



the resulting MMMs exhibited a high  $H_2$  to  $CO_2$  selectivity of 20.3 (Table 3). As opposed to conventional blending-based MMM fabrication, Park et al. applied polymer-modification-enabled in situ MOF formation (PMMOF) method to synthesize ZIF-7/PI MMMs [99]. The crystal phase of the ZIF-7 filler was tunable within the PI matrix, giving a phase III ZIF-7-based MMM with  $H_2$  permeability of 1630 barrer and  $H_2/CO_2$  selectivity of 3.8 (Figure 5).

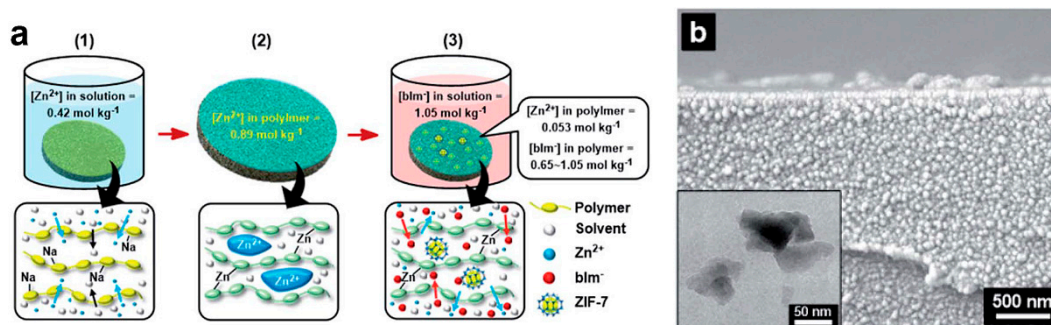


**Figure 5.** (a) Illustration of the in situ growth of ZIF-7 in PI matrix. (b) Scanning electron microscope image of the cross-section of the ZIF-7/PI MMM. The inset shows a transmission electron microscope image of the in situ formed phase III ZIF-7 fillers in the PI matrix. Reprinted with permission from ref. [99]. Copyright 2020 Royal Society of Chemistry.

To further enhance the polymer-filler interfacial compatibility, polydopamine can be used as a compatibilizing layer [100,101], which is typically coated onto MOF particles either by post-synthesis treatment or in situ polymerization during MOF synthesis. Wang et al. synthesized ZIF-8-PD by dispersing synthesized ZIF-8 nanocrystals into polydopamine precursor solution [102]. The coated ZIF-8-PD particles showed great compatibility with PI matrix, resulting in significant enhancement in gas permeability at almost no compromise in gas selectivity [102]. In comparison, Jiang et al. reported an in situ dopamine-modulated synthesis method to obtain monodispersed ZIF-8-DA particles in one step [103]. The incorporation of monodispersed ZIF-8-DA particles in Matrimid® 5218 membranes was able to demonstrate simultaneously improved  $H_2$  permeability and  $H_2/CO_2$  selectivity.

Compared to MOF nanoparticles, two-dimensional (2D) MOF nanosheets are more efficient fillers for MMMs since the partially oriented nanosheets with high-aspect-ratio will increase the chance of sieving the gas molecules [104–108]. ZIF-L is one of the most accessible 2D MOFs [109,110]. Kim et al. reported that the MMM containing 20 wt.% dopamine modified ZIF-L could get a 550% improvement in  $H_2/CO_2$  selectivity (from 1.7 to 13.4) (Table 3) [111]. Deng et al. synthesized two different types of ZIF-L with the selection of different metal sources, and revealed that ZIF-L-Co was better than ZIF-L-Zn in elevating the  $H_2$  permeability of MMMs [112]. MMM with 20% ZIF-L-Co showed the best  $H_2$  permeability at 1986 barrer. Bi et al. also incorporated ultrathin Co-benzenedicarboxylate MOF nanosheets (CBMNs) into a 6FDA-Durene-DABA matrix (Figure 6a), leading to improved  $H_2$  separation with a  $H_2/CH_4$  selectivity of up to 42 [113]. Recently, Ma et al. proposed a new concept of fabricating MMMs [85]. Instead of embedding the filler in the polymer matrix, the ZIF-7 nanosheets were oriented and penetrated through the PI matrix, given that the thickness of the ZIF-7 nanosheets was larger than the PI membrane (Figure 6b). Through this design, the channels of the penetrating ZIF-7 nanosheets served as the dominant pathways for gas molecules, resulting in extremely high molecular sieving performance observed for  $H_2$  separation. The  $H_2/CO_2$  and  $H_2/CH_4$  selectivity could reach 91.5 and 128.4, respectively, with a  $H_2$  permeance of  $3.0 \times 10^{-7} \text{ mol m}^{-2} \text{ s}^{-1} \text{ Pa}^{-1}$ . Despite the high promise of using MOF nanosheets in MMMs for  $H_2$  separation, one of the key challenges lies in the production of high-quality MOF nanosheets to support the large-scale membrane fabrication [114].

**Table 3.** Summary of representative performances for MOF-based membranes in H<sub>2</sub>-based separation.

Membrane			Separation Performance					Ref.
Filler	Polymer/Support	Test Condition	Permeation Area (cm <sup>2</sup> )	P(H <sub>2</sub> ) (GPU)	Selectivity			
					H <sub>2</sub> /CO <sub>2</sub>	H <sub>2</sub> /CH <sub>4</sub>	H <sub>2</sub> /N <sub>2</sub>	
CAU-1-NH <sub>2</sub> (15 wt%)	PMMA	3 bar, 25 °C	0.02	11,000 <sup>a</sup> (+122%)	13 (+333%)	-	-	[84]
CBMN (2 wt%)	6FDA-Durene-DABA	3 bar, 25 °C	-	410 <sup>a</sup> (−24%)	1.2 (−14%)	29 (+45%)	42 (+83%)	[113]
[Cu <sub>2</sub> (ndc) <sub>2</sub> (dabco)] <sub>n</sub> (30 wt%)	PBI	2 bar, 35 °C	-	12.1 <sup>a</sup> (+236%)	11 (+21%)	-	-	[104]
MIL-53(Al)-NH <sub>2</sub> (20 wt%)	PI-1388 (VTEC™)	5 bar, 35 °C	16	5.4 <sup>a</sup> (+8%)	5.4 (+8%)	-	-	[86]
NH <sub>2</sub> -CAU-1 (20 wt%)	PMMA with ceramic	2 bar	-	92 (+475%)	33 (+400%)	-	-	[87]
NH <sub>2</sub> -MIL-53 (20 wt%)	PMMA with ceramic	2 bar	-	72 (+350%)	45 (+582%)	-	-	[87]
nZIF-7	PEI	2 bar, 35 °C	-	1.1 (−45%)	3.2 (−68%)	42 (+324%)	54 (+38%)	[95]
PSM-nZIF-7	PEI	2 bar, 35 °C	-	8.6 (+330%)	9.9 (−1%)	23 (+132%)	13 (−67%)	[95]
UiO-66 (3 wt%)	PAA/PVP	-	-	1.2 (−56%)	20.3 (+62%)	-	-	[98]
UiO-66-NH <sub>2</sub> (55 wt%)	6FDA-DAM:DABA (3:2)	3 bar, 35 °C	-	2932 <sup>a</sup> (+1529%)	1.2 (+20%)	34 (+3%)	24 (+4%)	[89]
UiO-66-NH <sub>2</sub> (40 wt%)	6FDA-DAM	3 bar, 35 °C	-	1810 <sup>a</sup> (+165%)	0.7 (−13%)	10 (−29%)	10 (−23%)	[89]
UiO-66-NH <sub>2</sub> (40 wt%)	6FDA-BPDA-DAM (1:1)	3 bar, 35 °C	-	1086 <sup>a</sup> (+198%)	0.8 (+14%)	12 (+14%)	13 (+13%)	[89]
UiO-66-NH <sub>2</sub> (18 wt%)	PVP/PEI	1 bar, 25 °C	-	31 <sup>a</sup> (+244%)	0.08 (−81%)	-	-	[88]
UiO-66(Hf)-(OH) <sub>2</sub> (10 wt%)	PBI	2 bar, 35 °C	-	8.2 <sup>a</sup> (+128%)	12 (+33%)	-	-	[82]
Oriented & Penetrating ZIF-7	PI	2 bar, 100 °C	-	889 (+1357%) <sup>b</sup>	92 (+889%) <sup>b</sup>	-	128 (+1424%) <sup>b</sup>	[85]
ZIF-7-I	6FDA-DAM with α-alumina	-	-	921 <sup>a</sup> (+56%)	2 (+100%)	67 (+68%)	36 (+16%)	[99]
ZIF-7-III	6FDA-DAM with α-alumina	-	-	322 <sup>a</sup> (−45%)	4 (+300%)	172 (+330%)	59 (+90%)	[99]
ZIF-7-mix	6FDA-DAM with α-alumina	-	-	478 <sup>a</sup> (−45%)	4 (+300%)	86 (+115%)	32 (+3%)	[99]
ZIF-8 (5 wt%)	PSF	4 bar, 30 °C	-	53 <sup>a</sup> (+43%)	2.3 (+5%)	57 (+24%)	58 (+21%)	[100]
ZIF-8 (20 wt%)	6FDA-Durene	1 bar, 35 °C	-	1525 <sup>a</sup> (+80%)	1 (+11%)	16 (+11%)	14 (+18%)	[102]
ZIF-8-PD (20 wt%)	6FDA-Durene	1 bar, 35 °C	-	1320 <sup>a</sup> (+56%)	1 (+11%)	16 (+11%)	17 (0%)	[102]
ZIF-8 (40 wt%)	Matrimid® 5218	3.5 bar, 35 °C	-	400 <sup>a</sup> (+1329%)	4 (+33%)	50 (−52%)	44 (−50%)	[103]
ZIF-8-DA (40 wt%)	Matrimid® 5218	3.5 bar, 35 °C	-	65 <sup>a</sup> (+132%)	4 (+33%)	108 (+4%)	130 (+48%)	[103]
ZIF-8 (20 wt%)	TR polymers (90% conversion)	1 bar, 35 °C	3.14	1206 <sup>a</sup> (+189%)	1.3 (+30%)	28 (+22%)	21 (0%)	[97]
ZIF-93 (20 wt%)	PBI	3 bar, 180 °C	3.14	128 <sup>a</sup> (+184%)	5 (+25%)	-	-	[96]

Table 3. Cont.

Membrane			Separation Performance					Ref.
Filler	Polymer/Support	Test Condition	Permeation Area (cm <sup>2</sup> )	P(H <sub>2</sub> ) (GPU)	Selectivity			
					H <sub>2</sub> /CO <sub>2</sub>	H <sub>2</sub> /CH <sub>4</sub>	H <sub>2</sub> /N <sub>2</sub>	
ZIF-L (20 wt%)	PI	1 bar	-	260 <sup>a</sup> (+18%)	13 (+550%)	62 (−11%)	41 (+3%)	[111]
ZIF-L-Co (20 wt%)	TB	2 bar, 24 °C	-	1236 <sup>a</sup> (+312%)	2 (0%)	26 (+48%)	25 (−49%)	[112]
ZIF-L-Zn (20 wt%)	TB	2 bar, 24 °C	-	898 <sup>a</sup> (+199%)	2 (0%)	25 (+50%)	23 (−53%)	[112]

<sup>a</sup> Permeability reported in the units of barrer; <sup>b</sup> percentage enhancement calculated with respect to the conventional unoriented MMM. Numbers in the parentheses represent the percentage enhancements with respect to the pristine polymeric membranes; 6FDA, 4,4'-(hexafluoroisopropylidene)diphthalic anhydride; CBMN, co-benzenedicarboxylate MOF nanosheet; DAM, 2,4,6-triphenyl-*m*-phenylenediamine; DABA, 3,5-diaminobenzoic acid; ndc, 1,4-naphthalene dicarboxylate; dabco, 1,4-diazabicyclo(2.2.2)octane; ns, nanosheets; PAA, poly(acrylic acid); PBI, polybenzimidazole; PD, polydopamine; PEI, polyethyleneimine; PI, polyimide; PMMA, poly(methyl methacrylate); PPO, poly(phenylene oxide); PVP, polyvinylpyrrolidone; TB, Troger's base; TPIM, phenazine-containing triptycene ladder polymers; TR, thermally rearranged.

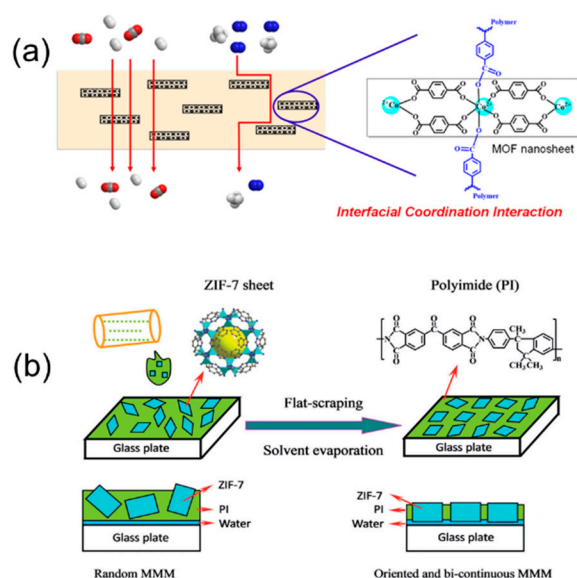


**Figure 6.** Illustration of (a) the 6FDA-Durene-DABA/CBMN MMM. Reprinted with permission from Ref. [113], Copyright 2020 American Chemical Society, and (b) a schematic showing the preparation of the oriented and penetrating ZIF-7@PI MMM. Reprinted with permission from ref. [85]. Copyright 2019 Wiley-VCH.

#### 4.3. COF-Based Membranes

COFs are a class of microporous organic polymers—joining porous aromatic frameworks (PAFs), conjugated microporous polymers (CMPs), and hyper-crosslinked polymers (HCPs) etc.—composed of light elements connected via covalent bonds [115–117]. Contrary to inorganic zeolites and organic-inorganic hybrid MOFs, COFs are purely organic, and have the natural advantage of good interfacial compatibility with organic polymers [118]. Moreover, the covalently bonded backbones of COFs endow these materials with a better chemical stability than MOFs, making them better filler materials for gas separation under harsh conditions. Similar to zeolites, the pore sizes of most COFs are too large to show any discriminatory sieving of H<sub>2</sub> from other gases. Therefore, nanolaminated COF membranes are always composited with other materials such as MOFs and GO to form dual-layer/composite membranes [119–122]. Another way to effectuate precise molecular sieving is to fabricate vertically aligned COF membranes to allow gas molecules to separate via the narrow nanochannels defined by the interlayer spacing between COF nanosheets [123]. However, due to the high cost and technical challenges in fabricating

these types of membranes, MMMs are still the preferential membrane type for COF-based membranes.

As an emerging filler material, COFs are frequently adopted to enhance the poor selectivity and physical aging resistance of highly permeable glassy polymers [124]. For example, the size-controlled HCPs were used to redeem the gas selectivity and the long-term stability of the ultra-permeable poly(1-trimethylsilyl-1-propyne) (PTMSP) membrane as reported by Hou et al. [125]. Owing to the sufficient HCP-PTMSP interaction and efficient dispersion of the HCP particles,  $H_2/CH_4$  and  $H_2/N_2$  selectivity were enhanced by 690% and 540%, reaching up to 22 and 30, respectively. The same group also added PAF-1 additives into the highly permeable TPIM-2 polymer matrix, leading to simultaneous improvement in the  $H_2$  permeability,  $H_2/N_2$  selectivity, and long-term stability of the MMM [126]. PAF-1 was also used to elevate the  $H_2$  separation performance of PIM-1 membranes. The addition of PAF-1 filler in PIM-1 not only improves the  $H_2$  permeability of the membrane to 5500 barrer (Table 4), but more importantly, also endows the MMM with a good physical aging resistance as exemplified by a higher  $H_2/N_2$  selectivity with age [127].

Similar to 2D MOFs, 2D COFs are equally attractive for MMMs. Many COFs have 2D laminar structures that can be easily exfoliated into high-aspect-ratio nanosheets for improving membrane selectivity [128,129]. For example, the incorporation of a type of 2D COF, named NUS-2 (Figure 7), at 20 wt.% loading in PBI matrix showed an improved  $H_2/CO_2$  selectivity from 9.5 to 31.4 with a slight improvement in  $H_2$  permeability (Table 4) [130].

**Table 4.** Summary of representative performances for COF-based membranes in  $H_2$ -based separation.

Membrane			Separation Performance					
Filler	Polymer/Support	Test Condition	Permeation Area (cm <sup>2</sup> )	P(H <sub>2</sub> ) (GPU)	Selectivity			Ref.
					H <sub>2</sub> /CO <sub>2</sub>	H <sub>2</sub> /CH <sub>4</sub>	H <sub>2</sub> /N <sub>2</sub>	
COF <sub>L</sub>	PVAm/mPSF	5 bar	-	90 (+221%)	0.1 (0%)	-	-	[131]
COF <sub>M</sub>	PVAm/mPSF	5 bar	-	85 (+204%)	0.085 (−15%)	-	-	[131]
COF <sub>P</sub>	PVAm/mPSF	5 bar	-	58 (+107%)	0.052 (−48%)	-	-	[131]
PAOPIM-1 (10 wt%)	PI-COOH	3 bar	-	1279 <sup>a</sup> (+3%)	1 (+11%)	16.7 (+14%)	23.5 (+22%)	[132]
NUS-2 (20 wt%)	Ultem	2 bar, 35 °C	-	22.7 <sup>a</sup> (+255%)	4.6 (+59%)	103 (+78%)	-	[130]
NUS-2 (20 wt%)	PBI	5 bar, 35 °C	-	4.1 <sup>a</sup> (+14%)	31.4 (+231%)	-	-	[130]
NUS-3 (20 wt%)	Ultem	2 bar, 35 °C	-	33.4 <sup>a</sup> (+423%)	2.2 (−24%)	63 (+9%)	-	[130]
NUS-3 (20 wt%)	PBI	5 bar, 35 °C	-	12.2 <sup>a</sup> (+239%)	8.9 (−6%)	-	-	[130]
<i>p</i> -DCX (10 wt%)	PTMSP	2 bar, 25 °C	-	30,000 <sup>a</sup> (+53%)	0.7 (+17%)	2.8 (0%)	5.0 (+4%)	[125]
V-125 (10 wt%)	PTMSP	2 bar, 25 °C	-	11,100 <sup>a</sup> (−43%)	0.7 (+17%)	4.3 (+54%)	7.6 (+62%)	[125]
PAF-1 (10 wt%)	PTMSP	2 bar, 25 °C	-	18,400 <sup>a</sup> (−6%)	0.7 (+17%)	4.8 (+72%)	8.3 (+77%)	[125]
PAF-1 (10 wt%)	TPIM-2	-	-	4886 <sup>a</sup> (+196%)	1 (+25%)	18.8 (+18%)	23.4 (+20%)	[126]
PAF-1 (10 wt%)	PIM-1	-	-	5500 <sup>a</sup> (+375%)	-	-	4.5 (+13%)	[127]

<sup>a</sup> Permeability reported in the units of barrer; numbers in the parentheses represent the percentage enhancements with respect to the pristine polymeric membranes; PI, polyimide; PIM-1, polymer of intrinsic microporosity; PSF, polysulfone; PVAm, polyvinylamine; TPIM, phenazine-containing triptycene ladder polymers.



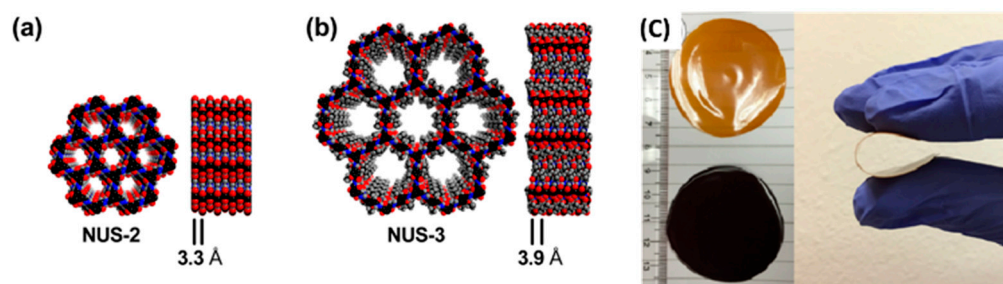


**Figure 7.** Crystal structures, showing a pore size of (a) NUS-2 as compared to (b) NUS-3, and (c) photo images of 20 wt %NUS-2@Ultem (brown) and 20 wt %NUS-3@Ultem (black). Reprinted with permission from ref. [130]. Copyright 2016 American Chemical Society.

Furthermore, given the rich chemistry and functional groups, the organic structure of COFs is an ideal platform to realize molecular level fusion with polymer matrix. Cao et al. grafted chemical functional groups, such as  $-\text{CHO}$  and  $-\text{NH}_2$ , and polymer segments of poly(vinyl amine) (PVAm) onto a 2D COF (COF-LZU1) before blending with the PVAm matrix (Figure 8) [131]. The results indicated that the MMMs incorporated with PVAm grafted COFs showed a reverse selectivity with  $\text{CO}_2/\text{H}_2$  selectivity highest at 22.2. Recently, Huang et al. developed an in situ generation strategy to synthesis polymer molecular sieve (PMS) within the polymer matrix, which can load as high as 70 wt.% PMS in the MMMs [132]. The obtained MMMs exhibited a high  $\text{H}_2/\text{CH}_4$  selectivity of 183.

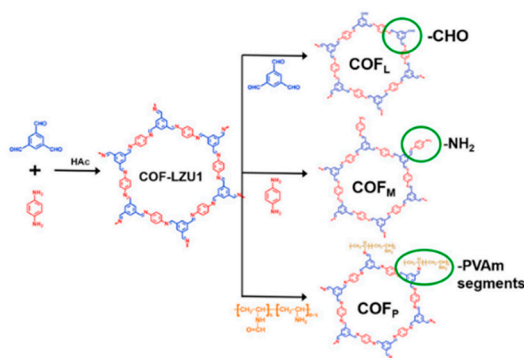


**Figure 8.** Synthesis process of functionalized  $\text{COF}_L$ ,  $\text{COF}_M$  and  $\text{COF}_P$ . Reprinted with permission from ref. [131]. Copyright 2020 Elsevier.

#### 4.4. Graphene-Based Membranes

Graphene consists of a single-layer  $sp^2$ -hybridized carbon atoms arranged in a hexagonal honey-comb lattice [133,134]. The applicability of graphene-based materials, especially GO, in membranes for gas separation has been an active area of research, owing to its 2D morphology and monoatomic thickness, which theoretically gives the lowest possible transport resistance. Castarlenas et al. demonstrated the potential utility of GO in PSF and Matrimid<sup>®</sup> 5218 polymer matrices for  $\text{H}_2$  separation [135] in which MMMs showed undesirable decrease in both  $\text{H}_2/\text{CH}_4$  selectivity ( $\sim 50\%$  and  $38\%$ , respectively) and  $\text{H}_2$  permeability ( $\sim 140\%$  and  $100\%$ , respectively) with increased GO loading from 4 wt% to 8 wt% (Figure 9a and Table 5). The decrease in  $\text{H}_2$  permeability stemmed from the nonporous nature of GO that resulted in gas diffusion taking up an extensively tortuous pathway across the membranes. Considering that  $\text{CH}_4$  possesses a higher polarizability than  $\text{H}_2$  [45], the decrease in  $\text{H}_2/\text{CH}_4$  selectivity may be attributed to the favorable interaction between  $\text{CH}_4$  and the functional groups on the GO. This is evidenced by the contradictory increase in mixed-gas  $\text{CO}_2/\text{CH}_4$  selectivity with increase in GO loading, suggesting the presence of strong GO interaction with the gas molecules [136,137]. Albeit the drop in  $\text{H}_2$  permeability with GO loading, graphene-based materials show a strong capacity for improving the mechanical properties of MMMs. For instance, 10 wt% loading of GO nanosheets in

Matrimid® 5218 matrix showcased more than 100% increment in the Young's modulus of the membranes [138].

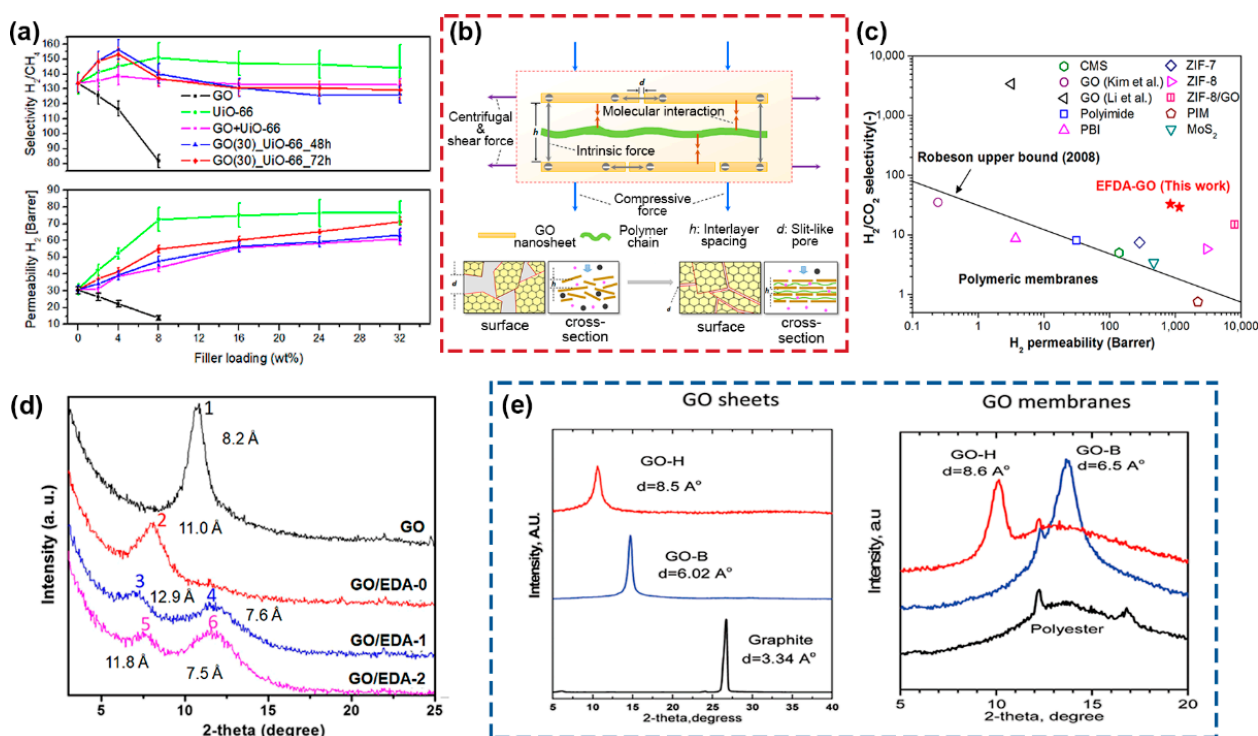


**Figure 9.** (a) Performance of mixed-matrix membranes containing graphene oxide (GO), showing GO, UiO-66 and UiO-66/GO effect on  $H_2$  permeability and  $H_2/CH_4$  selectivity in Matrimid® 5218 polymer matrix. Reprinted with permission from ref. [135]. Copyright 2017 Elsevier. (b) An illustration of the GO-laminated membrane intercalated by polyethyleneimine and (c) its  $H_2/CO_2$  performance with reference to the 2008 Robeson upper bound. Reprinted with permission from ref. [139]. Copyright 2016 American Chemical Society. (d) Comparison of the XRD profile and  $d$ -spacing between GO membranes and GO membranes intercalated with ethylenediamine (EDA). Reprinted with permission from ref. [140]. Copyright 2018 Elsevier. (e) Effects of two different GO synthesis methods (GO-H, GO synthesized by modified Hummer's method and GO-B, GO synthesized by modified Brodie's method) on the  $d$ -spacing of the GO sheets and laminated membranes. Reprinted with permission from ref. [141]. Copyright 2019 Royal Society of Chemistry.

On this account, GO can be designed as ultrathin laminates on top of polymeric membrane substrates to avoid excessive compromise in the membrane's gas permeability. GO-laminated membranes conduct molecular sieving by using the interlayer spacing between GO nanosheets that serves as well-defined nanochannel for molecular transport. Precise control of the size of the interlayer spacing is key to achieving selective gas transport and separation, and this feat can be realized by intercalating different spacers between GO nanosheets [133,142]. While laminated membranes deviate from the usual MMMs in which filler materials are mixed within dense matrices, the design and outcome are similar when polymeric spacers are used. Hence, we report only GO-laminated membranes that are intercalated by polymers to align with the scope of this review. Shen et al. assembled GO with 0.1 wt.% polyethyleneimine to fine-tune the interlayer spacing to within 0.4 nm [139]. By applying an external force driven assembly (EFDA) method comprising a vacuum-spin technique, they were able to obtain a highly ordered laminar structure (Figure 9b) that exhibited  $H_2$  permeability of between 840–1200 barrer and  $H_2/CO_2$  selectivity of between 29–33, surpassing the 2008 Robeson upper bound (Figure 9c and Table 5).

**Table 5.** Summary of representative performances for graphene-based membranes in H<sub>2</sub>-based separation.

Membrane		Separation Performance						Ref.
Filler	Polymer/Support	Test Condition	Permeation Area (cm <sup>2</sup> )	P(H <sub>2</sub> ) (GPU)	Selectivity			
					H <sub>2</sub> /CO <sub>2</sub>	H <sub>2</sub> /CH <sub>4</sub>	H <sub>2</sub> /N <sub>2</sub>	
CGO-76 (C=Cysteamine)	Anodized Al <sub>2</sub> O <sub>3</sub>	1.5 bar, 25 °C	3.14	52 (−45%) <sup>b</sup>	21 (+133%) <sup>b</sup>	-	-	[143]
GO (8 wt%)	PSF	35 °C	-	4.7 <sup>a</sup> (−61%)	-	29 (−51%)	-	[135]
GO (8 wt%)	PI	35 °C	-	14 <sup>a</sup> (−55%)	-	82 (−39%)	-	[135]
GO/PEI	Porous Al <sub>2</sub> O <sub>3</sub>	25 °C	3.14	1000 <sup>a</sup> (−83%)	29 (+625%)	-	-	[139]
GO/EDA-2	Porous Al <sub>2</sub> O <sub>3</sub>	25 °C	3.14	73 (−42%) <sup>b</sup>	23 (+35%)	-	-	[140]

<sup>a</sup> Permeability reported in the units of barrer; <sup>b</sup> percentage enhancement calculated with respect to pristine GO-laminated membranes; numbers in the parentheses represent the percentage enhancements with respect to the pristine polymeric membranes. PEI, polyethyleneimine; EDA-2, 2 h pre-crosslinking with ethylenediamine

Another study conducted by Lin et al. [140] utilized ethylenediamine (EDA) as the polymer spacer to fabricate GO-laminated membranes, given that EDA can be cross-linked to the −COOH groups on GO nanosheets. The cross-linking time between GO and EDA (GO/EDA-X where X = 0, 1 and 2 in hours) was varied, and two different stacking patterns were observed with the increase in cross-linking time (i.e., GO/EDA-1: *d*-spacing = 12.9 Å and 7.6 Å; GO/EDA-2: *d*-spacing = 11.8 Å and 7.5 Å), as opposed to GO/EDA-0, which possessed a single *d*-spacing of 11.0 Å (Figure 9d). The two types of stacking arose from: (1) an increase in the interlayer spacing due to the presence of EDA molecules, and (2) a decrease in interlayer spacing due to GO reduction by the EDA. Owing to these changes, a sharp decrease in H<sub>2</sub> permeance and an increase in H<sub>2</sub>/CO<sub>2</sub> selectivity were reported as compared to pure GO membrane. A similar investigation was also conducted by Cheng et al. [143] in which cysteamine, which contains both amino and thiol functional groups, cross-linked with GO nanosheets to give a smaller interlayer spacing that led to an enhancement in H<sub>2</sub>/CO<sub>2</sub> selectivity, reaching above 20 (Table 5).

On a different note, the interlayer spacing of GO nanosheets can also be tuned with the use of different synthesis methods. In general, the most common approach in GO synthesis is via a modified Hummers' method (GO-H), considering that this approach allows rapid graphite oxidation [144]. However, it is generally difficult for GO membranes made from this GO-H to possess an interlayer spacing that is smaller than 8 Å. As a demonstration, in the study conducted by Ibrahim et al. [141], GO membranes was assembled from GO synthesized using a modified Brodie's method (GO-B) [145]. GO-B gave GO-laminated membranes with smaller interlayer spacing (Figure 9e), and this resulted in a substantial increase in H<sub>2</sub>/CO<sub>2</sub>, H<sub>2</sub>/N<sub>2</sub> and H<sub>2</sub>/CH<sub>4</sub> selectivity of up to 129%, 91% and 76%, respectively, as compared to GO-H. However, GO synthesis via the modified Brodie's method is comparatively more complicated than the modified Hummer's method [144], as successive graphite oxidation is necessary to achieve the desired oxidation (i.e., C/O ratio > 2), and this added complexity should be considered for graphene-based membrane fabrication.

#### 4.5. Binary Fillers

As discussed in Section 4.4, using GO alone as a filler for MMMs is less effective due to its undesirable decrease in H<sub>2</sub> permeability. Thus, the use of binary fillers, which includes incorporating two separate fillers into the polymer matrix or combining two fillers into three-dimensional (3D) composites, has been demonstrated to be promising for enhancing H<sub>2</sub> separation performances [138,146]. For example, Castarlenas et al. [135] explored MMMs using two different types of filler: (1) a UiO-66/GO composite, and (2) individual UiO-66 and GO fillers physically blended into the polymer matrix. Enhancements in both

H<sub>2</sub> permeability and H<sub>2</sub>/CH<sub>4</sub> selectivity were observed when using UiO-66/GO composite as a filler material in Matrimid<sup>®</sup> 5218 (Figure 9a and Table 6), which was attributed to the improvement in polymer-filler interfacial adhesion brought by compositing the two fillers together. In contrast, physical blending UiO-66 and GO into the polymer matrix failed to achieve the same enhancements, as the individual fillers were unable to provide the same effective interfacial adhesion as that of the composite counterpart.

**Table 6.** Summary of representative performances for MMMs with binary fillers in H<sub>2</sub>-based separation.

Membrane		Separation Performance						Ref.
Filler	Polymer/Support	Test Condition	Permeation Area (cm <sup>2</sup> )	P(H <sub>2</sub> ) (GPU)	Selectivity			
					H <sub>2</sub> /CO <sub>2</sub>	H <sub>2</sub> /CH <sub>4</sub>	H <sub>2</sub> /N <sub>2</sub>	
UiO-66 + GO (8 wt%)	PSF	35 °C	-	12 <sup>a</sup> (0%)	-	60 (+2%)	-	[135]
UiO-66 + GO (8 wt%)	PI	35 °C	-	41 <sup>a</sup> (+32%)	-	136 (+1%)	-	[135]
MCM-41 + MIL-53(Al)-NH <sub>2</sub> (8 wt%)	PSF	35 °C	15.2	20 <sup>a</sup> (+67%)	-	67 (+14%)	-	[147]
MCM-41 + MIL-53(Al)-NH <sub>2</sub> (8 wt%)	PI	35 °C	15.2	16 <sup>a</sup> (−47%)	-	132 (0%)	-	[147]
MCM-41 + JDF-L1 (8 + 4 wt%)	6FDA-based copolyimide	35 °C	-	440 <sup>a</sup> (+41%)	-	32 (+68%)	-	[148]
HKUST-1 + Silicalite-1 (8 wt%)	PSF	35 °C	15.2	16 <sup>a</sup> (+33%)	-	83 (+38%)	-	[149]
ZIF-8 + Silicalite-1 (8 wt%)	PSF	35 °C	15.2	17 <sup>a</sup> (+42%)	-	74 (+23%)	-	[149]

<sup>a</sup> Permeability reported in the units of barrer; numbers in the parentheses represent the percentage enhancements with respect to the pristine polymeric membranes; 6FDA, 4,4'-(hexafluoroisopropylidene)diphthalic anhydride; PI, polyimide; PSF, polysulfone.

To ensure the success of the physical blending strategy, careful pairing of the fillers is important. For example, Valero et al. leveraged two different porous filler materials—an ordered mesoporous silica, MCM-41, and a MOF, MIL-53(Al)-NH<sub>2</sub>—in PSF matrix to improve filler dispersion and polymer-filler interfacial interaction [147]. They found that at 8 wt.% loading of each filler, MCM-41 was able to reduce MOF agglomeration, leading to tiny MIL-53(Al)-NH<sub>2</sub> particles surrounding the shell of the silica spheres. As a result, H<sub>2</sub>/CH<sub>4</sub> selectivity of the MMM was enhanced by 14%, reaching 67.3, while improving the H<sub>2</sub> permeability by 67% (Table 6) [147]. The enhancements were attributed to the synergistic effect brought by the mesoporosity of MCM-41 as well as the microporosity and chemical compatibility of MIL-53(Al)-NH<sub>2</sub> to the polymer matrix. Another attractive approach to achieving synergistic enhancements is to blend a 2D material to complement a 3D filler. Galve et al. used a JDF-L1 layered titanosilicate to pair with calcined MCM-41 3D spheres in a 6FDA-based copolyimide matrix for MMM preparation [148]. Owing to the strong barrier effect of the layered JDF-L1, H<sub>2</sub>/CH<sub>4</sub> selectivity was able to enhance by 88%. At an optimal loading of 8 wt.% MCM-41 and 4 wt.% JDF-1, the H<sub>2</sub> permeability was able to reach 440 barrer at H<sub>2</sub>/CH<sub>4</sub> selectivity of 32.0, which corresponded to a 41% and 68% enhancement in permeability and selectivity, respectively (Table 6) [148].

## 5. Critical Evaluation of Hydrogen Separation Performances

On the basis of the discussions made in Section 4, we have summarized the H<sub>2</sub> separation performances of representative MMMs in the recent literature (Tables 2–6). Here, a direct comparison of the separation performances across MMMs of different filler categories is hardly possible, given that the testing conditions, such as applied pressure, temperature, filler loading, and the use between single- and mixed-gas evaluations, are all not comparable. Nevertheless, certain trends are in general unambiguous. First, MOFs are



seemingly the most common choice of filler, owing to their microporosity, and versatile chemical functionality that enables strong interfacial adhesion to the polymer matrix. Second, broadly speaking, 2D filler materials such as graphene-based materials and COFs tend to produce higher membrane selectivity, as a result of their high-aspect-ratios, leading to gas diffusion undertaking a more tortuous pathway through the polymer matrix. Third, although the binary filler strategy boasts synergistic enhancements in both permeability and selectivity, its true value lies more in minimizing loss in membrane selectivity, either through creating better polymer-filler interfacial interaction or the use of 2D materials to extend the transport pathway. As such, most MMMs with binary fillers show moderate to high membrane selectivity as compared to single-filler MMMs (Table 6). Here, we want to emphasize that the undesirable incompatibility between filler and polymer (e.g., sieve-in-a-cage, rigidified interface and plugged sieves) remains one of the Achilles' heels of MMMs, which can deteriorate membrane performances and cause the MMM strategy to backfire [44]. Hence, it is important to consider the physicochemical properties when choosing filler materials and fine-tune them for unlocking the true potential of MMMs. Fourth, most of the studies in Tables 2–6 did not report the permeation area of their membranes, and for those who did, the areas were typically in the scale of a few to tens of centimeters. There are clearly little efforts thus far to demonstrate the potential of scaling-up MMMs (see our discussion on scalability in Section 6). Last but not least, it is evident from the data that the intrinsic separation performance of the polymer matrix plays an active role in determining the performance outcome of the MMMs. For example, using an intrinsically high-permeable 6FDA-based polymer will ensure that the H<sub>2</sub> permeability is high to start with, and hard to outperform by MMMs using low-permeable PSF and PI matrices, albeit permeability enhancements by the filler materials (see binary filler of Table 6). Hence, it is important to have a deep understanding of the intrinsic performance of polymer matrices, to allow rational pairing of filler materials with positive enhancements that complement the polymer matrices, for surpassing the H<sub>2</sub> Robeson upper bounds (see Figure 3).

## 6. Conclusions and Perspectives

To conclude, we presented an overview of the current hydrogen market, focusing especially on existing technologies for hydrogen generation and purification, and how membrane separation can add value and contribute toward the future hydrogen economy. However, delivering the promise of membrane separation necessitates the evaluation of the current performance of polymeric membranes. Hence, in this review, we featured MMMs as one of the most compelling strategies to date, and singled out emerging filler materials, including zeolites, MOFs, COFs, and graphene-based materials, which we believe could change the game for MMMs. Further discussions on these fillers were first conducted, correlating the effects of physicochemical properties, such as porosity, morphology, and chemistry, on the polymer-filler interfacial interaction, and the ensuing H<sub>2</sub> separation performances of the MMMs. Then, we examined the binary filler strategy and gained perspective on how two filler materials can create synergistic permeability-selectivity enhancements. A critical evaluation on the H<sub>2</sub> separation performance data also provided key lessons learned for readers to take away from representative MMMs from these filler categories.

H<sub>2</sub> membrane separation is in general challenging due to the fast diffusivity and low solubility of H<sub>2</sub> molecules, leading to poor discrimination toward other penetrant gas molecules. Hence, moving forward, we argue that future development should focus on molecular-level tailoring of filler materials through fine-tuning porosity for increasing the molecular sieving capacity. This feat can be achieved by pre-synthetic engineering of the ligands or the strut length of the monomers used for MOF and COF syntheses, respectively. Alternatively, post-synthetic chemical functionalization of the pores can be used to create more constricted and well-defined pore sizes to target specifically H<sub>2</sub> separation. On the same note, H<sub>2</sub> molecules having fast diffusivity also demand a tighter polymer-filler

interfacial morphology to mitigate defective MMMs. This therefore calls for optimized filler loadings, better dispersibility to prevent excessive agglomeration and greater interfacial compatibility through customizing the surface chemistry.

In addition, H<sub>2</sub> separation under industrial relevant conditions typically involve high temperature as well as pressure. For example, the syngas produced by WGS reaction, following SMR, can have a temperature as high as above 200 °C [33], and stay at a pressure of at least 5–10 bar and beyond [150]. Hence, we suppose that future work on MMMs for H<sub>2</sub> separation should place a stronger emphasis on membrane performances under elevated temperature and pressure. This includes demonstrating the thermal stability of the filler materials and the polymer matrices as well as understanding the optimal filler loadings to render robust mechanical properties of the MMMs to handle the applied pressure by the feed gas. As shown in Tables 2–6, there is currently scarce literature on H<sub>2</sub> separation by MMMs at elevated temperatures, partly due to safety concerns and the availability of only a handful of polymeric materials with high glass transition temperatures. Moreover, there is a need to demonstrate chemical stability of filler materials and MMMs toward detrimental impurities in feed gases such as water, acidic gases and sulfur containing species [33]. Thus, taken together, these gaps need to be better addressed to provide a more accurate evaluation of MMMs in overcoming the permeability-selectivity tradeoff of polymeric membranes.

In terms of pairing filler materials to polymer matrices, there is a growing interest from the membrane community to see rational pairing for more meaningful designs of MMMs. As previously discussed, rational pairing involves the exploitation of specific attributes of filler materials to complement the limitations of polymer matrices (see Section 5). For example, Thür et al. recently found that the CO<sub>2</sub> adsorption enthalpy ( $Q_{st}$ ) of MOF-808 gave a stronger correlation to the performance of MMMs as opposed to its intrinsic CO<sub>2</sub> uptake, suggesting a possibility of thoughtful design of MOF-based MMMs by leveraging proven structural-performance indicators [151]. Furthermore, considering that the polymer matrices have a strong influence over the MMM performance (see discussion in Section 5), our group recently attempted to decouple the polymer matrix effect, and proposed a filler enhancement index ( $F_{index}$ ) that illuminates the true effectiveness of the filler by considering both permeability and selectivity enhancements for CO<sub>2</sub>/CH<sub>4</sub> separation [44]. This index allows filler materials to be rated using a single composite metric for easy screening of polymer matrices to find the best match for pairing. In this age in which data represents a competitive edge, making data-driven decisions using these approaches is highly appealing and serves to meet the needs of rationally-designed MMMs for H<sub>2</sub> separation.

Finally, demonstrating the scalability of MMMs is yet another milestone that demands a stronger commitment from both the industry and academia. Current research on MMMs for H<sub>2</sub> separation are geared toward performance enhancements, without placing considerable effort into scaling-up MMMs to a scale that is practical for pilot-testing or test-bedding, as evidenced by the lack of information or small permeation areas as highlighted in Tables 2–6. Conversely, without crucial data such as this, there is limited buy-in from the industry, leaving MMMs a slow-to-adopt technology despite decades of academic research. Hence, for the academia, we call for greater efforts in translational research, such as scaling-up of MMMs for pilot-scale H<sub>2</sub> separation evaluations as well as test-bedding, to showcase higher technology readiness level (TRL). Life-cycle assessments and techno-economic reviews should also be undertaken to provide more holistic assessments of the potential of MMMs for H<sub>2</sub> separation. As for the industry, it is important to work collectively with academia by introducing more ground for exploration, feedback and co-creation such that academic research can stay relevant to the needs of the H<sub>2</sub> market. We believe that it is only through collective and collaborative efforts such as these that the gaps for MMMs can be closed and technology transfer from laboratories to the market be successfully administered. With the impending hydrogen economy, demonstrating higher TRL and lowering the barrier for rationally-designed MMMs to reach commercialization

will unquestionably strengthen the competitive position of membrane technology for H<sub>2</sub> separation.

**Author Contributions:** Conceptualization, K.G. writing—original draft preparation, C.Y.C. and X.J.; writing—review and editing, K.G.; supervision, R.W.; funding acquisition, R.W. All authors have read and agreed to the published version of the manuscript.

**Funding:** We would like to thank the Singapore Economic Development Board (EDB) for funding support to Singapore Membrane Technology Centre.

**Institutional Review Board Statement:** Not applicable.

**Informed Consent Statement:** Not applicable.

**Data Availability Statement:** Not applicable.

**Conflicts of Interest:** The authors declare no conflict of interest.

## References

- Ahmad, T.; Zhang, D. A critical review of comparative global historical energy consumption and future demand: The story told so far. *Energy Rep.* **2020**, *6*, 1973–1991. [CrossRef]
- Jamil, M.; Ahmad, F.; Jeon, Y.J. Renewable energy technologies adopted by the UAE: Prospects and challenges—A comprehensive overview. *Renew. Sustain. Energy Rev.* **2016**, *55*, 1181–1194. [CrossRef]
- World Economic Forum. *Nature and Net Zero*; The World Economic Forum in collaboration with McKinsey & Company, World Economic Forum: Geneva, Switzerland, 2021.
- Zerta, M.; Schmidt, P.R.; Stiller, C.; Landinger, H. Alternative World Energy Outlook (AWE0) and the role of hydrogen in a changing energy landscape. *Int. J. Hydrogen Energy* **2008**, *33*, 3021–3025. [CrossRef]
- Friedlander, B. Touted as Clean, ‘Blue’ Hydrogen May Be Worse Than Gas or Coal. Available online: <https://news.cornell.edu/stories/2021/08/touted-clean-blue-hydrogen-may-be-worse-gas-or-coal> (accessed on 15 July 2021).
- Atilhan, S.; Park, S.; El-Halwagi, M.M.; Atilhan, M.; Moore, M.; Nielsen, R.B. Green hydrogen as an alternative fuel for the shipping industry. *Curr. Opin. Chem. Eng.* **2021**, *31*, 100668. [CrossRef]
- van Renssen, S. The hydrogen solution? *Nat. Clim. Chang.* **2020**, *10*, 799–801. [CrossRef]
- Noussan, M.; Raimondi, P.P.; Scita, R.; Hafner, M. The role of green and blue hydrogen in the energy transition—A technological and geopolitical perspective. *Sustainability* **2021**, *13*, 298. [CrossRef]
- DiChristopher, T. Experts Explain Why Green Hydrogen Costs Have Fallen and Will Keep Falling. Available online: <https://www.spglobal.com/marketintelligence/en/news-insights/latest-news-headlines/experts-explain-why-green-hydrogen-costs-have-fallen-and-will-keep-falling-63037203> (accessed on 12 July 2020).
- Collins, L. A Wake-Up Call on Green Hydrogen: The Amount of Wind and Solar Needed Is Immense. Available online: <https://www.rechargenews.com/transition/a-wake-up-call-on-green-hydrogen-the-amount-of-wind-and-solar-needed-is-immense/2-1-776481> (accessed on 12 July 2021).
- Hulst, N.v. The Clean Hydrogen Future Has Already Begun. Available online: <https://www.iea.org/commentaries/the-clean-hydrogen-future-has-already-begun> (accessed on 12 July 2020).
- Shao, L.; Low, B.T.; Chung, T.-S.; Greenberg, A.R. Polymeric membranes for the hydrogen economy: Contemporary approaches and prospects for the future. *J. Membr. Sci.* **2009**, *327*, 18–31. [CrossRef]
- Shu, L.; Xie, L.-H.; Meng, Y.; Liu, T.; Zhao, C.; Li, J.-R. A thin and high loading two-dimensional MOF nanosheet based mixed-matrix membrane for high permeance nanofiltration. *J. Membr. Sci.* **2020**, *603*, 118049. [CrossRef]
- Park, S.; Jeong, H.-K. Transforming polymer hollow fiber membrane modules to mixed-matrix hollow fiber membrane modules for propylene/propane separation. *J. Membr. Sci.* **2020**, *612*, 118429. [CrossRef]
- Barooah, M.; Mandal, B. Synthesis, characterization and CO<sub>2</sub> separation performance of novel PVA/PG/ZIF-8 mixed matrix membrane. *J. Membr. Sci.* **2019**, *572*, 198–209. [CrossRef]
- Robeson, L.M. Correlation of separation factor versus permeability for polymeric membranes. *J. Membr. Sci.* **1991**, *62*, 165–185. [CrossRef]
- Robeson, L.M. The upper bound revisited. *J. Membr. Sci.* **2008**, *320*, 390–400. [CrossRef]
- Li, W.; Goh, K.; Chuah, C.Y.; Bae, T.-H. Mixed-matrix carbon molecular sieve membranes using hierarchical zeolite: A simple approach towards high CO<sub>2</sub> permeability enhancements. *J. Membr. Sci.* **2019**, *588*, 117220. [CrossRef]
- Chuah, C.Y.; Lee, J.; Bae, T.-H. Graphene-based membranes for H<sub>2</sub> separation: Recent progress and future perspective. *Membranes* **2020**, *10*, 336. [CrossRef] [PubMed]
- Giancarlo, T. *Hydrogen Production & Distribution*; International Energy Agency-Energy Technology System Analysis Programme: USA, 2014. Available online: [https://iea-etsap.org/E-TechDS/PDF/P12\\_H2\\_Feb2014\\_FINAL%203\\_CRES-2a-GS%20Mz%20GSOK.pdf](https://iea-etsap.org/E-TechDS/PDF/P12_H2_Feb2014_FINAL%203_CRES-2a-GS%20Mz%20GSOK.pdf) (accessed on 12 July 2020).

21. Liu, K.; Song, C.; Subramani, V. *Hydrogen and Syngas Production and Purification Technologies*; John Wiley & Sons: Hoboken, NJ, USA, 2010.
22. Robert, R. Life Cycle Emissions of Hydrogen. Available online: <https://4thgeneration.energy/life-cycles-emissions-of-hydrogen/> (accessed on 14 January 2021).
23. IEA. The Future of Hydrogen. Available online: <https://www.iea.org/reports/the-future-of-hydrogen> (accessed on 14 January 2021).
24. Angeli, S.D.; Monteleone, G.; Giaconia, A.; Lemonidou, A.A. State-of-the-art catalysts for CH<sub>4</sub> steam reforming at low temperature. *Int. J. Hydrogen Energy* **2014**, *39*, 1979–1997. [CrossRef]
25. Meloni, E.; Martino, M.; Palma, V. A short review on Ni based catalysts and related engineering issues for methane steam reforming. *Catalysts* **2020**, *10*, 352. [CrossRef]
26. Salameh, Z. *Renewable Energy System Design*; Academic Press: Cambridge, MA, USA, 2014.
27. Energy Efficiency & Renewable Energy. Hydrogen Production: Biomass Gasification. Available online: <https://www.energy.gov/eere/fuelcells/hydrogen-production-biomass-gasification#:~:text=Biomass%20gasification%20is%20a%20mature,and%20other%20products%2C%20without%20combustion> (accessed on 28 June 2021).
28. Sikarwar, V.S.; Zhao, M.; Clough, P.; Yao, J.; Zhong, X.; Memon, M.Z.; Shah, N.; Anthony, E.J.; Fennell, P.S. An overview of advances in biomass gasification. *Energy Environ. Sci.* **2016**, *9*, 2939–2977. [CrossRef]
29. Brauns, J.; Turek, T. Alkaline water electrolysis powered by renewable energy: A review. *Processes* **2020**, *8*, 248. [CrossRef]
30. Kumar, S.S.; Himabindu, V. Hydrogen production by PEM water electrolysis—A review. *Mater. Sci. Energy Technol.* **2019**, *2*, 442–454.
31. Zeng, K.; Zhang, D. Recent progress in alkaline water electrolysis for hydrogen production and applications. *Prog. Energy Combust. Sci.* **2010**, *36*, 307–326. [CrossRef]
32. Maric, R.; Yu, H. Proton exchange membrane water electrolysis as a promising technology for hydrogen production and energy storage. In *Nanostructures in Energy Generation, Transmission and Storage*; IntechOpen: London, UK, 2019; p. 13.
33. Ockwig, N.W.; Nenoff, T.M. Membranes for hydrogen separation. *Chem. Rev.* **2007**, *107*, 4078–4110. [CrossRef]
34. Chuah, C.Y.; Lee, Y.; Bae, T.-H. Potential of adsorbents and membranes for SF<sub>6</sub> capture and recovery: A review. *Chem. Eng. J.* **2020**, *404*, 126577. [CrossRef]
35. Sircar, S.; Golden, T. *Pressure Swing Adsorption Technology for Hydrogen Production*; John Wiley & Sons: Hoboken, NJ, USA, 2010.
36. Linde. *Hydrogen Recovery by Pressure Swing Adsorption*; Linde AG: Pullach, Germany, 2021.
37. Li, W.; Chuah, C.Y.; Yang, Y.; Bae, T.-H. Nanocomposites formed by in situ growth of NiDOBDC nanoparticles on graphene oxide sheets for enhanced CO<sub>2</sub> and H<sub>2</sub> storage. *Micropor. Mesopor. Mater.* **2018**, *265*, 35–42. [CrossRef]
38. Al-Mufachi, N.; Rees, N.; Steinberger-Wilkens, R. Hydrogen selective membranes: A review of palladium-based dense metal membranes. *Renew. Sustain. Energy Rev.* **2015**, *47*, 540–551. [CrossRef]
39. Aasadnia, M.; Mehrpooya, M.; Ghorbani, B. A novel integrated structure for hydrogen purification using the cryogenic method. *J. Clean. Prod.* **2020**, *278*, 123872. [CrossRef]
40. Terrien, P.; Lockwood, F.; Granados, L.; Morel, T. CO<sub>2</sub> capture from H<sub>2</sub> plants: Implementation for EOR. *Energy Procedia* **2014**, *63*, 7861–7866. [CrossRef]
41. Airliquide. *CRYOCAPT™: Cryogenic Solution for CO<sub>2</sub> Capture, a World Premiere*; Airliquide: Paris, France, 2015; p. 12.
42. Schorer, L.; Schmitz, S.; Weber, A. Membrane based purification of hydrogen system (MEMPHYS). *Int. J. Hydrogen Energy* **2019**, *44*, 12708–12714. [CrossRef]
43. Bernardo, G.; Araújo, T.; da Silva Lopes, T.; Sousa, J.; Mendes, A. Recent advances in membrane technologies for hydrogen purification. *Int. J. Hydrogen Energy* **2020**, *45*, 7313–7338. [CrossRef]
44. Chuah, C.Y.; Goh, K.; Yang, Y.; Gong, H.; Li, W.; Karahan, H.E.; Guiver, M.D.; Wang, R.; Bae, T.-H. Harnessing filler materials for enhancing biogas separation membranes. *Chem. Rev.* **2018**, *118*, 8655–8769. [CrossRef]
45. Li, J.-R.; Kuppler, R.J.; Zhou, H.-C. Selective gas adsorption and separation in metal–organic frameworks. *Chem. Soc. Rev.* **2009**, *38*, 1477–1504. [CrossRef]
46. Chuah, C.Y.; Kim, K.; Lee, J.; Koh, D.-Y.; Bae, T.-H. CO<sub>2</sub> absorption using membrane contactors: Recent progress and future perspective. *Ind. Eng. Chem. Res.* **2019**, *59*, 6773–6794. [CrossRef]
47. Chuah, C.Y.; Li, W.; Samarasinghe, S.; Sethunga, G.; Bae, T.-H. Enhancing the CO<sub>2</sub> separation performance of polymer membranes via the incorporation of amine-functionalized HKUST-1 nanocrystals. *Micropor. Mesopor. Mater.* **2019**, *290*, 109680. [CrossRef]
48. Peramanu, S.; Cox, B.; Pruden, B. Economics of hydrogen recovery processes for the purification of hydroprocessor purge and off-gases. *Int. J. Hydrogen Energy* **1999**, *24*, 405–424. [CrossRef]
49. Goh, K.; Jiang, W.; Karahan, H.E.; Zhai, S.; Wei, L.; Yu, D.; Fane, A.G.; Wang, R.; Chen, Y. All-carbon nanoarchitectures as high-performance separation membranes with superior stability. *Adv. Funct. Mater.* **2015**, *25*, 7348–7359. [CrossRef]
50. Yang, E.; Alayande, A.B.; Goh, K.; Kim, C.-M.; Chu, K.-H.; Hwang, M.-H.; Ahn, J.-H.; Chae, K.-J. 2D materials-based membranes for hydrogen purification: Current status and future prospects. *Int. J. Hydrogen Energy* **2021**, *46*, 11389–11410. [CrossRef]
51. Wong, K.C.; Goh, P.S.; Ismail, A.F. Enhancing hydrogen gas separation performance of thin film composite membrane through facilely blended polyvinyl alcohol and PEBAX. *Int. J. Hydrogen Energy* **2021**, *46*, 19737–19748. [CrossRef]
52. Noble, R.D. Perspectives on mixed matrix membranes. *J. Membr. Sci.* **2011**, *378*, 393–397. [CrossRef]



53. Qian, S.; Xia, L.; Yang, L.; Wang, X.; Suo, X.; Cui, X.; Xing, H. Defect-free mixed-matrix membranes consisting of anion-pillared metal-organic frameworks and poly(ionic liquid)s for separation of acetylene from ethylene. *J. Membr. Sci.* **2020**, *611*, 118329. [[CrossRef](#)]
54. Zhao, Y.; Jung, B.T.; Ansaloni, L.; Ho, W.W. Multiwalled carbon nanotube mixed matrix membranes containing amines for high pressure CO<sub>2</sub>/H<sub>2</sub> separation. *J. Membr. Sci.* **2014**, *459*, 233–243. [[CrossRef](#)]
55. Ismail, A.; Goh, P.; Sanip, S.; Aziz, M. Transport and separation properties of carbon nanotube-mixed matrix membrane. *Sep. Purif. Technol.* **2009**, *70*, 12–26. [[CrossRef](#)]
56. Swaidan, R.; Ghanem, B.; Pinnau, I. Fine-tuned intrinsically ultramicroporous polymers redefine the permeability/selectivity upper bounds of membrane-based air and hydrogen separations. *ACS Macro Lett.* **2015**, *4*, 947–951. [[CrossRef](#)]
57. Ding, L.; Wei, Y.; Li, L.; Zhang, T.; Wang, H.; Xue, J.; Ding, L.-X.; Wang, S.; Caro, J.; Gogotsi, Y. MXene molecular sieving membranes for highly efficient gas separation. *Nat. Commun.* **2018**, *9*, 1–7. [[CrossRef](#)] [[PubMed](#)]
58. Wu, A.X.; Drayton, J.A.; Smith, Z.P. The perfluoropolymer upper bound. *AIChE J.* **2019**, *65*, e16700. [[CrossRef](#)]
59. Bastani, D.; Esmaeili, N.; Asadollahi, M. Polymeric mixed matrix membranes containing zeolites as a filler for gas separation applications: A review. *J. Ind. Eng. Chem.* **2013**, *19*, 375–393. [[CrossRef](#)]
60. Kosinov, N.; Gascon, J.; Kapteijn, F.; Hensen, E.J.M. Recent developments in zeolite membranes for gas separation. *J. Membr. Sci.* **2016**, *499*, 65–79. [[CrossRef](#)]
61. Morris, R.E.; Wheatley, P.S. Gas storage in nanoporous materials. *Angew. Chem. Int. Ed.* **2008**, *47*, 4966–4981. [[CrossRef](#)]
62. Lee, S.; Kim, B.; Kim, J. Predicting performance limits of methane gas storage in zeolites with an artificial neural network. *J. Mater. Chem. A* **2019**, *7*, 2709–2716. [[CrossRef](#)]
63. Chuah, C.Y.; Goh, K.; Bae, T.-H. Enhanced performance of carbon molecular sieve membranes incorporating zeolite nanocrystals for air separation. *Membranes* **2021**, *11*, 489. [[CrossRef](#)]
64. Mei, W.; Du, Y.; Wu, T.; Gao, F.; Wang, B.; Duan, J.; Zhou, J.; Zhou, R. High-flux CHA zeolite membranes for H<sub>2</sub> separations. *J. Membr. Sci.* **2018**, *565*, 358–369. [[CrossRef](#)]
65. Zhou, M.; Korelskiy, D.; Ye, P.; Grah, M.; Hedlund, J. A uniformly oriented MFI membrane for improved CO<sub>2</sub> separation. *Angew. Chem. Int. Ed.* **2014**, *126*, 3560–3563. [[CrossRef](#)]
66. Yu, L.; Nobandegani, M.; Hedlund, J. High performance fluoride MFI membranes for efficient CO<sub>2</sub>/H<sub>2</sub> separation. *J. Membr. Sci.* **2020**, *616*, 118623. [[CrossRef](#)]
67. Hu, L.; Cheng, J.; Li, Y.; Liu, J.; Zhang, L.; Zhou, J.; Cen, K. Composites of ionic liquid and amine-modified SAPO 34 improve CO<sub>2</sub> separation of CO<sub>2</sub>-selective polymer membranes. *Appl. Surf. Sci.* **2017**, *410*, 249–258. [[CrossRef](#)]
68. Peydayesh, M.; Mohammadi, T.; Bakhtiari, O. Effective hydrogen purification from methane via polyimide Matrimid®5218-deca-dodecasil 3R type zeolite mixed matrix membrane. *Energy* **2017**, *141*, 2100–2107. [[CrossRef](#)]
69. Ahmad, J.; Hägg, M.-B. Preparation and characterization of polyvinyl acetate/zeolite 4A mixed matrix membrane for gas separation. *J. Membr. Sci.* **2013**, *427*, 73–84. [[CrossRef](#)]
70. Rezakazemi, M.; Shahidi, K.; Mohammadi, T. Sorption properties of hydrogen-selective PDMS/zeolite 4A mixed matrix membrane. *Int. J. Hydrogen Energy* **2012**, *37*, 17275–17284. [[CrossRef](#)]
71. Esmaeili, N.; Boyd, S.E.; Brown, C.L.; Mac, A. Gray, E.; Webb, C.J. Improving the gas-separation properties of PVAc-zeolite 4A mixed-matrix membranes through nano-sizing and silanation of the zeolite. *ChemPhysChem* **2019**, *20*, 1590–1606. [[CrossRef](#)]
72. Eden, C.L.; Daramola, M.O. Evaluation of silica sodalite infused polysulfone mixed matrix membranes during H<sub>2</sub>/CO<sub>2</sub> separation. *Mater. Today Proc.* **2021**, *38*, 522–527. [[CrossRef](#)]
73. Hu, C.-C.; Cheng, P.-H.; Chou, S.-C.; Lai, C.-L.; Huang, S.-H.; Tsai, H.-A.; Hung, W.-S.; Lee, K.-R. Separation behavior of amorphous amino-modified silica nanoparticle/polyimide mixed matrix membranes for gas separation. *J. Membr. Sci.* **2020**, *595*, 117542. [[CrossRef](#)]
74. Miricioiu, M.G.; Iacob, C.; Nechifor, G.; Niculescu, V.-C. High Selective Mixed Membranes Based on Mesoporous MCM-41 and MCM-41-NH<sub>2</sub> Particles in a Polysulfone Matrix. *Front. Chem.* **2019**, *7*, 332. [[CrossRef](#)]
75. Wang, X.; Ding, X.; Zhao, H.; Fu, J.; Xin, Q.; Zhang, Y. Pebax-based mixed matrix membranes containing hollow polypyrrole nanospheres with mesoporous shells for enhanced gas permeation performance. *J. Membr. Sci.* **2020**, *602*, 117968. [[CrossRef](#)]
76. Tseng, H.-H.; Chuang, H.-W.; Zhuang, G.-L.; Lai, W.-H.; Wey, M.-Y. Structure-controlled mesoporous SBA-15-derived mixed matrix membranes for H<sub>2</sub> purification and CO<sub>2</sub> capture. *Int. J. Hydrogen Energy* **2017**, *42*, 11379–11391. [[CrossRef](#)]
77. Zornoza, B.; Esekhi, O.; Koros, W.J.; Téllez, C.; Coronas, J. Hollow silicalite-1 sphere-polymer mixed matrix membranes for gas separation. *Sep. Purif. Technol.* **2011**, *77*, 137–145. [[CrossRef](#)]
78. Zornoza, B.; Téllez, C.; Coronas, J.; Esekhi, O.; Koros, W.J. Mixed matrix membranes based on 6FDA polyimide with silica and zeolite microsphere dispersed phases. *AIChE J.* **2015**, *61*, 4481–4490. [[CrossRef](#)]
79. Zhou, H.C.; Long, J.R.; Yaghi, O.M. Introduction to metal-organic frameworks. *Chem. Rev.* **2012**, *112*, 673–674. [[CrossRef](#)] [[PubMed](#)]
80. Seoane, B.; Coronas, J.; Gascon, I.; Etcheberria Benavides, M.; Karvan, O.; Caro, J.; Kapteijn, F.; Gascon, J. Metal-organic framework based mixed matrix membranes: A solution for highly efficient CO<sub>2</sub> capture? *Chem. Soc. Rev.* **2015**, *44*, 2421–2454. [[CrossRef](#)]
81. Denny, M.S.; Moreton, J.C.; Benz, L.; Cohen, S.M. Metal-organic frameworks for membrane-based separations. *Nat. Rev. Mater.* **2016**, *1*, 16078. [[CrossRef](#)]

82. Hu, Z.; Kang, Z.; Qian, Y.; Peng, Y.; Wang, X.; Chi, C.; Zhao, D. Mixed matrix membranes containing UiO-66(Hf)-(OH)<sub>2</sub> metal-organic framework nanoparticles for efficient H<sub>2</sub>/CO<sub>2</sub> separation. *Ind. Eng. Chem. Res.* **2016**, *55*, 7933–7940. [\[CrossRef\]](#)
83. Lin, R.; Villacorta Hernandez, B.; Ge, L.; Zhu, Z. Metal organic framework based mixed matrix membranes: An overview on filler/polymer interfaces. *J. Mater. Chem. A* **2018**, *6*, 293–312. [\[CrossRef\]](#)
84. Cao, L.; Tao, K.; Huang, A.; Kong, C.; Chen, L. A highly permeable mixed matrix membrane containing CAU-1-NH<sub>2</sub> for H<sub>2</sub> and CO<sub>2</sub> separation. *Chem. Commun.* **2013**, *49*, 8513–8515. [\[CrossRef\]](#)
85. Ma, X.; Wu, X.; Caro, J.; Huang, A. Polymer composite membrane with penetrating ZIF-7 sheets displays high hydrogen permselectivity. *Angew. Chem. Int. Ed.* **2019**, *131*, 16302–16306. [\[CrossRef\]](#)
86. Perez, E.V.; Kalaw, G.J.D.; Ferraris, J.P.; Balkus, K.J.; Musselman, I.H. Amine-functionalized (Al) MIL-53/VTEC™ mixed-matrix membranes for H<sub>2</sub>/CO<sub>2</sub> mixture separations at high pressure and high temperature. *J. Membr. Sci.* **2017**, *530*, 201–212. [\[CrossRef\]](#)
87. Zhao, Y.; Zhao, D.; Kong, C.; Zhou, F.; Jiang, T.; Chen, L. Design of thin and tubular MOFs-polymer mixed matrix membranes for highly selective separation of H<sub>2</sub> and CO<sub>2</sub>. *Sep. Purif. Technol.* **2019**, *220*, 197–205. [\[CrossRef\]](#)
88. Ashtiani, S.; Khoshnamvand, M.; Bouša, D.; Šturala, J.; Sofer, Z.; Shaliutina-Kolešová, A.; Gardenö, D.; Friess, K. Surface and interface engineering in CO<sub>2</sub>-philic based UiO-66-NH<sub>2</sub>-PEI mixed matrix membranes via covalently bridging PVP for effective hydrogen purification. *Int. J. Hydrogen Energy* **2021**, *46*, 5449–5458. [\[CrossRef\]](#)
89. Ma, C.; Urban, J.J. Hydrogen-bonded polyimide/metal-organic framework hybrid membranes for ultrafast separations of multiple gas pairs. *Adv. Funct. Mater.* **2019**, *29*, 1903243. [\[CrossRef\]](#)
90. Smith, S.J.D.; Ladewig, B.P.; Hill, A.J.; Lau, C.H.; Hill, M.R. Post-synthetic Ti exchanged UiO-66 metal-organic frameworks that deliver exceptional gas permeability in mixed matrix membranes. *Sci. Rep.* **2015**, *5*, 7823. [\[CrossRef\]](#) [\[PubMed\]](#)
91. Ahmad, M.Z.; Navarro, M.; Lhotka, M.; Zornoza, B.; Téllez, C.; de Vos, W.M.; Benes, N.E.; Konnertz, N.M.; Visser, T.; Semino, R.; et al. Enhanced gas separation performance of 6FDA-DAM based mixed matrix membranes by incorporating MOF UiO-66 and its derivatives. *J. Membr. Sci.* **2018**, *558*, 64–77. [\[CrossRef\]](#)
92. Lee, J.; Satheeshkumar, C.; Yu, H.J.; Kim, S.; Lee, J.S.; Seo, M.; Kim, M. Pore engineering of covalently connected metal-organic framework nanoparticle-mixed-matrix membrane composites for molecular separation. *ACS Appl. Nano Mater.* **2020**, *3*, 9356–9362. [\[CrossRef\]](#)
93. Zhu, H.; Wang, L.; Jie, X.; Liu, D.; Cao, Y. Improved interfacial affinity and CO<sub>2</sub> separation performance of asymmetric mixed matrix membranes by incorporating [ostmodified MIL-53(Al). *ACS Appl. Mater. Interfaces* **2016**, *8*, 22696–22704. [\[CrossRef\]](#)
94. Smith, S.J.D.; Konstas, K.; Lau, C.H.; Gozukara, Y.M.; Easton, C.D.; Mulder, R.J.; Ladewig, B.P.; Hill, M.R. Post-synthetic annealing: Linker self-exchange in UiO-66 and its effect on polymer-metal organic framework interaction. *Cryst. Growth Des.* **2017**, *17*, 4384–4392. [\[CrossRef\]](#)
95. Al-Maythaly, B.A.; Alloush, A.M.; Faizan, M.; Dafallah, H.; Elgzoly, M.A.A.; Seliman, A.A.A.; Al-Ahmed, A.; Yamani, Z.H.; Habib, M.A.M.; Cordova, K.E.; et al. Tuning the interplay between selectivity and permeability of ZIF-7 mixed matrix membranes. *ACS Appl. Mater. Interfaces* **2017**, *9*, 33401–33407. [\[CrossRef\]](#)
96. Sánchez-Laínez, J.; Zornoza, B.; Orsi, A.F.; Łozińska, M.M.; Dawson, D.M.; Ashbrook, S.E.; Francis, S.M.; Wright, P.A.; Benoit, V.; Llewellyn, P.L.; et al. Synthesis of ZIF-93/11 hybrid nanoparticles via post-synthetic modification of ZIF-93 and their use for H<sub>2</sub>/CO<sub>2</sub> separation. *Chem. A Eur. J.* **2018**, *24*, 11211–11219. [\[CrossRef\]](#)
97. Kim, J.S.; Moon, S.J.; Wang, H.H.; Kim, S.; Lee, Y.M. Mixed matrix membranes with a thermally rearranged polymer and ZIF-8 for hydrogen separation. *J. Membr. Sci.* **2019**, *582*, 381–390. [\[CrossRef\]](#)
98. Xiang, F.; Marti, A.M.; Hopkinson, D.P. Layer-by-layer assembled polymer/MOF membrane for H<sub>2</sub>/CO<sub>2</sub> separation. *J. Membr. Sci.* **2018**, *556*, 146–153. [\[CrossRef\]](#)
99. Park, S.; Cho, K.Y.; Jeong, H.-K. Polyimide/ZIF-7 mixed-matrix membranes: Understanding the in situ confined formation of the ZIF-7 phases inside a polymer and their effects on gas separations. *J. Mater. Chem. A* **2020**, *8*, 11210–11217. [\[CrossRef\]](#)
100. Mei, X.; Yang, S.; Lu, P.; Zhang, Y.; Zhang, J. Improving the Selectivity of ZIF-8/polysulfone-mixed matrix membranes by polydopamine modification for H<sub>2</sub>/CO<sub>2</sub> separation. *Front. Chem.* **2020**, *8*, 528. [\[CrossRef\]](#)
101. Zhang, W.; Ying, Y.; Ma, J.; Guo, X.; Huang, H.; Liu, D.; Zhong, C. Mixed matrix membranes incorporated with polydopamine-coated metal-organic framework for dehydration of ethylene glycol by pervaporation. *J. Membr. Sci.* **2017**, *527*, 8–17. [\[CrossRef\]](#)
102. Wang, Z.; Wang, D.; Zhang, S.; Hu, L.; Jin, J. Interfacial Design of Mixed Matrix Membranes for Improved Gas Separation Performance. *Adv. Mater.* **2016**, *28*, 3399–3405. [\[CrossRef\]](#) [\[PubMed\]](#)
103. Jiang, X.; He, S.; Han, G.; Long, J.; Li, S.; Lau, C.H.; Zhang, S.; Shao, L. Aqueous One-Step Modulation for Synthesizing Monodispersed ZIF-8 Nanocrystals for Mixed-Matrix Membrane. *ACS Appl. Mater. Interfaces* **2021**, *13*, 11296–11305. [\[CrossRef\]](#) [\[PubMed\]](#)
104. Kang, Z.; Peng, Y.; Hu, Z.; Qian, Y.; Chi, C.; Yeo, L.Y.; Tee, L.; Zhao, D. Mixed matrix membranes composed of two-dimensional metal-organic framework nanosheets for pre-combustion CO<sub>2</sub> capture: A relationship study of filler morphology versus membrane performance. *J. Mater. Chem. A* **2015**, *3*, 20801–20810. [\[CrossRef\]](#)
105. Cheng, Y.; Wang, X.; Jia, C.; Wang, Y.; Zhai, L.; Wang, Q.; Zhao, D. Ultrathin mixed matrix membranes containing two-dimensional metal-organic framework nanosheets for efficient CO<sub>2</sub>/CH<sub>4</sub> separation. *J. Membr. Sci.* **2017**, *539*, 213–223. [\[CrossRef\]](#)
106. Sabetghadam, A.; Liu, X.; Gottmer, S.; Chu, L.; Gascon, J.; Kapteijn, F. Thin mixed matrix and dual layer membranes containing metal-organic framework nanosheets and Polyactive™ for CO<sub>2</sub> capture. *J. Membr. Sci.* **2019**, *570–571*, 226–235. [\[CrossRef\]](#)

107. Peng, Y.; Li, Y.; Ban, Y.; Jin, H.; Jiao, W.; Liu, X.; Yang, W. Metal-organic framework nanosheets as building blocks for molecular sieving membranes. *Science* **2014**, *346*, 1356–1359. [[CrossRef](#)] [[PubMed](#)]
108. Rodenas, T.; Luz, I.; Prieto, G.; Seoane, B.; Miro, H.; Corma, A.; Kapteijn, F.; Llabrés i Xamena, F.X.; Gascon, J. Metal-organic framework nanosheets in polymer composite materials for gas separation. *Nat. Mater.* **2014**, *14*, 48. [[CrossRef](#)]
109. Şahin, F.; Topuz, B.; Kalıpçılar, H. Synthesis of ZIF-7, ZIF-8, ZIF-67 and ZIF-L from recycled mother liquors. *Micropor. Mesopor. Mater.* **2018**, *261*, 259–267. [[CrossRef](#)]
110. Chen, R.; Yao, J.; Gu, Q.; Smeets, S.; Baerlocher, C.; Gu, H.; Zhu, D.; Morris, W.; Yaghi, O.M.; Wang, H. A two-dimensional zeolitic imidazolate framework with a cushion-shaped cavity for CO<sub>2</sub> adsorption. *Chem. Commun.* **2013**, *49*, 9500–9502. [[CrossRef](#)]
111. Kim, S.; Shamsaei, E.; Lin, X.; Hu, Y.; Simon, G.P.; Seong, J.G.; Kim, J.S.; Lee, W.H.; Lee, Y.M.; Wang, H. The enhanced hydrogen separation performance of mixed matrix membranes by incorporation of two-dimensional ZIF-L into polyimide containing hydroxyl group. *J. Membr. Sci.* **2018**, *549*, 260–266. [[CrossRef](#)]
112. Deng, J.; Dai, Z.; Deng, L. H<sub>2</sub>-selective Troger's base polymer based mixed matrix membranes enhanced by 2D MOFs. *J. Membr. Sci.* **2020**, *610*, 118262. [[CrossRef](#)]
113. Bi, X.; Zhang, Y.; Zhang, F.; Zhang, S.; Wang, Z.; Jin, J. MOF nanosheet-based mixed matrix membranes with metal-organic coordination interfacial interaction for gas separation. *ACS Appl. Mater. Interfaces* **2020**, *12*, 49101–49110. [[CrossRef](#)] [[PubMed](#)]
114. Zhao, M.; Huang, Y.; Peng, Y.; Huang, Z.; Ma, Q.; Zhang, H. Two-dimensional metal-organic framework nanosheets: Synthesis and applications. *Chem. Soc. Rev.* **2018**, *47*, 6267–6295. [[CrossRef](#)]
115. Yuan, S.; Li, X.; Zhu, J.; Zhang, G.; Van Puyvelde, P.; Van der Bruggen, B. Covalent organic frameworks for membrane separation. *Chem. Soc. Rev.* **2019**, *48*, 2665–2681. [[CrossRef](#)]
116. Duan, K.; Wang, J.; Zhang, Y.; Liu, J. Covalent organic frameworks (COFs) functionalized mixed matrix membrane for effective CO<sub>2</sub>/N<sub>2</sub> separation. *J. Membr. Sci.* **2019**, *572*, 588–595. [[CrossRef](#)]
117. Yang, Y.; Chuah, C.Y.; Nie, L.; Bae, T.-H. Enhancing the mechanical strength and CO<sub>2</sub>/CH<sub>4</sub> separation performance of polymeric membranes by incorporating amine-appended porous polymers. *J. Membr. Sci.* **2019**, *569*, 149–156. [[CrossRef](#)]
118. Zou, X.; Zhu, G. Microporous Organic Materials for Membrane-Based Gas Separation. *Adv. Mater.* **2018**, *30*, 1700750. [[CrossRef](#)] [[PubMed](#)]
119. Das, S.; Ben, T.; Qiu, S.; Valtchev, V. Two-dimensional COF–three-dimensional MOF dual-layer membranes with unprecedentedly high H<sub>2</sub>/CO<sub>2</sub> selectivity and ultrahigh gas permeabilities. *ACS Appl. Mater. Interfaces* **2020**, *12*, 52899–52907. [[CrossRef](#)] [[PubMed](#)]
120. Fu, J.; Das, S.; Xing, G.; Ben, T.; Valtchev, V.; Qiu, S. Fabrication of COF-MOF composite membranes and their highly selective separation of H<sub>2</sub>/CO<sub>2</sub>. *J. Am. Chem. Soc.* **2016**, *138*, 7673–7680. [[CrossRef](#)] [[PubMed](#)]
121. Fan, H.; Peng, M.; Strauss, I.; Mundstock, A.; Meng, H.; Caro, J. MOF-in-COF molecular sieving membrane for selective hydrogen separation. *Nat. Commun.* **2021**, *12*, 38. [[CrossRef](#)] [[PubMed](#)]
122. Tang, Y.; Feng, S.; Fan, L.; Pang, J.; Fan, W.; Kong, G.; Kang, Z.; Sun, D. Covalent organic frameworks combined with graphene oxide to fabricate membranes for H<sub>2</sub>/CO<sub>2</sub> separation. *Sep. Purif. Technol.* **2019**, *223*, 10–16. [[CrossRef](#)]
123. Fan, H.; Peng, M.; Strauss, I.; Mundstock, A.; Meng, H.; Caro, J. High-flux vertically aligned 2D covalent organic framework membrane with enhanced hydrogen separation. *J. Am. Chem. Soc.* **2020**, *142*, 6872–6877. [[CrossRef](#)]
124. Yang, Y.; Goh, K.; Weerachanchai, P.; Bae, T.-H. 3D covalent organic framework for morphologically induced high-performance membranes with strong resistance toward physical aging. *J. Membr. Sci.* **2019**, *574*, 235–242. [[CrossRef](#)]
125. Hou, R.; O'Loughlin, R.; Ackroyd, J.; Liu, Q.; Doherty, C.M.; Wang, H.; Hill, M.R.; Smith, S.J.D. Greatly enhanced gas selectivity in mixed-matrix membranes through size-controlled hyper-cross-linked polymer additives. *Ind. Eng. Chem. Res.* **2020**, *59*, 13773–13782. [[CrossRef](#)]
126. Hou, R.; Ghanem, B.S.; Smith, S.J.D.; Doherty, C.M.; Setter, C.; Wang, H.; Pinnau, I.; Hill, M.R. Highly permeable and selective mixed-matrix membranes for hydrogen separation containing PAF-1. *J. Mater. Chem. A* **2020**, *8*, 14713–14720. [[CrossRef](#)]
127. Lau, C.H.; Konstas, K.; Thornton, A.W.; Liu, A.C.; Mudie, S.; Kennedy, D.F.; Howard, S.C.; Hill, A.J.; Hill, M.R. Gas-separation membranes loaded with porous aromatic frameworks that improve with age. *Angew. Chem. Int. Ed.* **2015**, *54*, 2669–2673. [[CrossRef](#)]
128. Berlanga, I.; Ruiz-González, M.L.; González-Calbet, J.M.; Fierro, J.L.G.; Mas-Ballesté, R.; Zamora, F. Delamination of Layered Covalent Organic Frameworks. *Small* **2011**, *7*, 1207–1211. [[CrossRef](#)] [[PubMed](#)]
129. Bunck, D.N.; Dichtel, W.R. Bulk Synthesis of exfoliated two-dimensional polymers using hydrazone-linked covalent organic frameworks. *J. Am. Chem. Soc.* **2013**, *135*, 14952–14955. [[CrossRef](#)] [[PubMed](#)]
130. Kang, Z.; Peng, Y.; Qian, Y.; Yuan, D.; Addicoat, M.A.; Heine, T.; Hu, Z.; Tee, L.; Guo, Z.; Zhao, D. Mixed matrix membranes (MMMs) comprising exfoliated 2D covalent organic frameworks (COFs) for efficient CO<sub>2</sub> separation. *Chem. Mater.* **2016**, *28*, 1277–1285. [[CrossRef](#)]
131. Cao, X.; Xu, H.; Dong, S.; Xu, J.; Qiao, Z.; Zhao, S.; Wang, J.; Wang, Z. Preparation of high-performance and pressure-resistant mixed matrix membranes for CO<sub>2</sub>/H<sub>2</sub> separation by modifying COF surfaces with the groups or segments of the polymer matrix. *J. Membr. Sci.* **2020**, *601*, 117882. [[CrossRef](#)]
132. Huang, M.; Wang, Z.; Lu, K.; Fang, W.; Bi, X.; Zhang, Y.; Jin, J. In-situ generation of polymer molecular sieves in polymer membranes for highly selective gas separation. *J. Membr. Sci.* **2021**, *630*, 119302. [[CrossRef](#)]
133. Goh, K.; Karahan, H.E.; Wei, L.; Bae, T.-H.; Fane, A.G.; Wang, R.; Chen, Y. Carbon nanomaterials for advancing separation membranes: A strategic perspective. *Carbon* **2016**, *109*, 694–710. [[CrossRef](#)]

134. Yang, E.; Goh, K.; Chuah, C.Y.; Wang, R.; Bae, T.-H. Asymmetric mixed-matrix membranes incorporated with nitrogen-doped graphene nanosheets for highly selective gas separation. *J. Membr. Sci.* **2020**, *615*, 118293. [\[CrossRef\]](#)
135. Castarlenas, S.; Téllez, C.; Coronas, J. Gas separation with mixed matrix membranes obtained from MOF UiO-66-graphite oxide hybrids. *J. Membr. Sci.* **2017**, *526*, 205–211. [\[CrossRef\]](#)
136. Li, W.; Samarasinghe, S.A.S.C.; Bae, T.-H. Enhancing CO<sub>2</sub>/CH<sub>4</sub> separation performance and mechanical strength of mixed-matrix membrane via combined use of graphene oxide and ZIF-8. *J. Ind. Eng. Chem.* **2018**, *67*, 156–163. [\[CrossRef\]](#)
137. Goh, K.; Karahan, H.E.; Yang, E.; Bae, T.-H. Graphene-based membranes for CO<sub>2</sub>/CH<sub>4</sub> separation: Key challenges and perspectives. *Appl. Sci.* **2019**, *9*, 2784. [\[CrossRef\]](#)
138. Li, W.; Chuah, C.Y.; Nie, L.; Bae, T.-H. Enhanced CO<sub>2</sub>/CH<sub>4</sub> selectivity and mechanical strength of mixed-matrix membrane incorporated with NiDOBDC/GO composite. *J. Ind. Eng. Chem.* **2019**, *74*, 118–125. [\[CrossRef\]](#)
139. Shen, J.; Liu, G.; Huang, K.; Chu, Z.; Jin, W.; Xu, N. Subnanometer two-dimensional graphene oxide channels for ultrafast gas Sieving. *ACS Nano* **2016**, *10*, 3398–3409. [\[CrossRef\]](#)
140. Lin, H.; Liu, R.; Dangwal, S.; Kim, S.-J.; Mehra, N.; Li, Y.; Zhu, J. Permselective H<sub>2</sub>/CO<sub>2</sub> separation and desalination of hybrid GO/rGO membranes with controlled pre-cross-linking. *ACS Appl. Mater. Interfaces* **2018**, *10*, 28166–28175. [\[CrossRef\]](#)
141. Ibrahim, A.F.; Banihashemi, F.; Lin, Y. Graphene oxide membranes with narrow inter-sheet galleries for enhanced hydrogen separation. *Chem. Commun.* **2019**, *55*, 3077–3080. [\[CrossRef\]](#)
142. Xin, Q.; Ma, F.; Zhang, L.; Wang, S.; Li, Y.; Ye, H.; Ding, X.; Lin, L.; Zhang, Y.; Cao, X. Interface engineering of mixed matrix membrane via CO<sub>2</sub>-philic polymer brush functionalized graphene oxide nanosheets for efficient gas separation. *J. Membr. Sci.* **2019**, *586*, 23–33. [\[CrossRef\]](#)
143. Cheng, L.; Guan, K.; Liu, G.; Jin, W. Cysteamine-crosslinked graphene oxide membrane with enhanced hydrogen separation property. *J. Membr. Sci.* **2020**, *595*, 117568. [\[CrossRef\]](#)
144. Nie, L.; Chuah, C.Y.; Bae, T.H.; Lee, J.M. Graphene-based advanced membrane applications in organic solvent nanofiltration. *Adv. Funct. Mater.* **2020**, *31*, 2006949. [\[CrossRef\]](#)
145. Brodie, B.C., XIII. On the atomic weight of graphite. *Phil. Trans. R. Soc.* **1859**, *149*, 249–259.
146. Samarasinghe, S.; Chuah, C.Y.; Yang, Y.; Bae, T.-H. Tailoring CO<sub>2</sub>/CH<sub>4</sub> separation properties of mixed-matrix membranes via combined use of two-and three-dimensional metal-organic frameworks. *J. Membr. Sci.* **2018**, *557*, 30–37. [\[CrossRef\]](#)
147. Valero, M.; Zornoza, B.; Téllez, C.; Coronas, J. Mixed matrix membranes for gas separation by combination of silica MCM-41 and MOF NH<sub>2</sub>-MIL-53(Al) in glassy polymers. *Micropor. Mesopor. Mater.* **2014**, *192*, 23–28. [\[CrossRef\]](#)
148. Galve, A.; Sieffert, D.; Staudt, C.; Ferrando, M.; Güell, C.; Téllez, C.; Coronas, J. Combination of ordered mesoporous silica MCM-41 and layered titanosilicate JDF-L1 fillers for 6FDA-based copolyimide mixed matrix membranes. *J. Membr. Sci.* **2013**, *431*, 163–170. [\[CrossRef\]](#)
149. Zornoza, B.; Seoane, B.; Zamaro, J.M.; Téllez, C.; Coronas, J. Combination of MOFs and zeolites for mixed-matrix membranes. *ChemPhysChem* **2011**, *12*, 2781–2785. [\[CrossRef\]](#)
150. Lin, H.; He, Z.; Sun, Z.; Vu, J.; Ng, A.; Mohammed, M.; Knief, J.; Merkel, T.C.; Wu, T.; Lambrecht, R.C. CO<sub>2</sub>-selective membranes for hydrogen production and CO<sub>2</sub> capture—Part I: Membrane development. *J. Membr. Sci.* **2014**, *457*, 149–161. [\[CrossRef\]](#)
151. Thür, R.; Van Havere, D.; Van Velthoven, N.; Smolders, S.; Lamine, A.; Wieme, J.; Van Speybroeck, V.; De Vos, D.; Vankelecom, I.F.J. Correlating MOF-808 parameters with mixed-matrix membrane (MMM) CO<sub>2</sub> permeation for a more rational MMM development. *J. Mater. Chem. A* **2021**, *9*, 12782–12796. [\[CrossRef\]](#)